THE SCATTER OF FAST NEUTRAL PARTICLES IN A GAS TARGET

by

Byron Lee Johnson

B.S., Louisiana Polytechnic Institute
(1958)

SUBMITTED IN PARTIAL FULFILLMENT OF THE
REQUIREMENTS FOR THE DEGREE OF
MASTER OF SCIENCE

at the

MASSACHUSETTS INSTITUTE OF TECHNOLOGY
June, 1960

Signature redacted

Signature of Author. . . . . .
Department of Electrical Engineering
May 9, 1960

Signature redacted

Certified by . . .
Thesis Supervisor

Signature redacted

Accepted by. . .
Chairman, Departmental Committee on Graduate Students

THE SCATTER OF FAST NEUTRAL PARTICLES IN A GAS TARGET

by

Byron Lee Johnson

Submitted to the Department of Electrical Engineering on May 9, 1960 in partial fulfillment of the requirements for the degree of Master of Science.

ABSTRACT

The scattering of a beam of particles undergoing charge transfer collisions in a gas target has been examined with emphasis on the factors relevant to the design of a source of fast neutral particles.

Incident particles of helium, neon, and argon were used with targets of hydrogen, helium, neon, and argon gas over an energy range of 20 to 40 kev. An equation giving the number of neutral particles as a function of angular dispersion has been developed and constants determined for its energy dependence. An example of the computation of an equation giving the gas target thickness for maximum neutral particles in a specific cone angle is made for the He-He process at 20 and 40 kev. Curves giving the maximum percentage of neutrals available as a function of cone angle is given for the He-He process at 20 and 40 kev.

No published results have been found with which to compare the experimental data but a method of obtaining capture cross sections from the scatter data is discussed and comparison with published results is shown to give reasonable agreement.

Thesis Supervisor: John G. Trump
Title: Professor of Electrical Engineering

Thesis Supervisor: Sanborn F. Philp
Title: Division of Sponsored Research

ACKNOWLEDGMENT

The author wishes to thank Professor John G. Trump and Dr. Sanborn F. Philp for suggesting this research topic and their guidance throughout the experiment. The help received from all the personnel of the High Voltage Research Laboratory is greatly appreciated.

This work was made possible by a generous grant from the National Science Foundation.

TABLE OF CONTENTS

LIST OF FIGURES

CHAPTER I

INTRODUCTION

In 1911 Dunayer discovered that thermal velocity molecular beams could be produced by methods similar to those used in collimating light.[1] The techniques of the molecular beam were extensively developed by Stern and his co-workers[2] between 1920 and 1933 into an accurate research tool.

The splitting of a beam of thermal velocity silver atoms by a inhomogeneous magnetic field, observed by Stern and Gerlach[3], verified experimentally the space quantization of angular momentum which had already been postulated in order to account for atomic spectra. The wave nature of thermal velocity particles was demonstrated by Estermann, Frisch, and Stern[4] verifying the de Broglie relation. The resonance method, introduced by Rabi[5], has enabled researchers to use the molecular beam to measure many of the electric and magnetic properties of atoms, molecules and nuclei.

Scattering of molecular beams of thermal velocities provides information concerning intermolecular forces at relatively large distances. At these velocities attraction forces are usually greater than the repulsive forces.[6] For information about intermolecular forces at small distances where the dominate force is repulsive, beams of higher velocities than could be produced thermally were needed.

Oliphant[7] was the first to produce a beam of fast neutral atoms. He found a beam of neutral metastable helium atoms while studying beams

of positive ions. Beeck[8] produced a beam of fast argon atoms by the charge transfer process of transferring an electron from a target atom to the incident positive ion to form a fast neutral atom. This charge transfer process has been the subject of numerous investigations. Much data is available on the capture and loss cross sections for many target materials and incident particles.[9]

Since fast neutral beams have become available much work has been done in the measuring of collision cross sections. With this data meaningful potential energy information can be obtained together with a greater insight into the theory of molecular binding. Other studies of the scatter of neutral beams have been confined to stopping power experiments, X-ray production, and the passing of a beam of particles through a window.

Recently, focused beams of fast neutral particles have become interesting and very helpful tools for the scientist to work with. Their great usefulness comes from the fact that they are unaffected by either electric or magnetic fields. This feature will allow researchers to use them for measuring purposes where the use of an ion beam would be impossible.

Of particular interest at this time is the injection of particles in the magnetic bottle containers of thermonuclear fusion experiments. When a sustained thermonuclear fusion reaction is a reality, a method of supplying the fusion elements must be devised. A focused beam of fast deuterium atoms could be shot into the reaction area. There the atom would be instantly ionized and become part of the plasma trapped

in the magnetic bottle. If the neutral beam is very intense there is a possibility that a small number of the atoms could pass through without being ionized and trapped. If so, a measure of their intensity and amount of scatter should give indications of the properties of the plasma.

Another special use of neutral beams is for the injection of particles into certain accelerators. There is now available a tandem particle accelerator produced by High Voltage Engineering Corporation which makes use of one high voltage Van de Graff machine to obtain two stages of acceleration. This is accomplished by accelerating a beam of negative ions to the terminal which is positive, there "stripping" them of electrons in a gas or thin foil target to form positive ions which are then accelerated from the terminal back to ground potential.

An additional stage of acceleration has been visualized by adding an additional high voltage terminal of negative potential. A beam of neutral particles could drift to this terminal, be formed into negative ions by charge transfer collisions in a gas target, and be accelerated to the positive terminal where they would be stripped and accelerated back to ground potential as in the present tandem accelerator. This would give a singly charged particle an energy of three times the terminal potential whereas the present tandem gives an energy of two times the terminal potential.

To design a feasible machine to do this, information must be known about the scatter or angular dispersion of a neutral beam as a function of energy, incident particle mass, gas target particle mass, and gas

target thickness. Information of this nature is not available at the present time from the literature.

It is the purpose of this investigation to attempt to find experimentally the relation between the scatter of the neutral beam and the four parameters mentioned.

The theoretical considerations of multiple scattering are so involved that no attempt will be made to correlate the experimental results to theory except in the case of very thin targets where only single scattering can be presumed to take place.

The only practical method of producing intense beams of well-focused neutral particles at the present time is by the charge transfer method. With this method relatively intense neutral beams that are fairly well-focussed may be obtained with energies from a few kev to several hundred kev with an optimum of from 30 - 50 kev. This method is the only one considered in this investigation.

CHAPTER II

FORMATION AND SCATTERING OF NEUTRALS

2.1 Charge Exchange Process

The process in the gas target can be described in the following manner. Using helium for an example; the particles have two charge states (0, 1) corresponding to the neutral atom and the singly charged positive ion. As the ratio of He^- to He^+ in the beam is less than 10^{-3}[15] and the doubly charged helium ion was not seen in this experiment He^- and He^{++} will be neglected in this treatment of the charge exchange process.

If we let ϕ_i be the fraction of the beam in charge state i after passing through an equilibrium gas target thickness (electron loss and electron capture reactions are equal) then

$$\phi_0 = \frac{\sigma_{10}}{\sigma_{01} + \sigma_{10}} \qquad \phi_1 = \frac{\sigma_{01}}{\sigma_{01} + \sigma_{10}}$$

where σ_{if} is the cross section for transfer from an initial state i to a final state f. The ratio for the cross section between states is

$$\frac{\phi_0}{\phi_1} = \frac{\sigma_{10}}{\sigma_{01}}$$

and the differential equations for the change in the flux of particles in the i state are

$$\frac{dn_0}{dx} = n_1 \sigma_{10} - n_0 \sigma_{01} \qquad (2.1\ a)$$

$$\frac{dn_1}{dx} = n_0 \sigma_{01} - n_1 \sigma_{10} \qquad (2.1\ b)$$

We can solve these equations and obtain the relationship

$$\frac{n_0}{N} = \phi_0 \left[1 - e^{-\eta x (\sigma_{01} + \sigma_{10})} \right] \qquad (2.2)$$

where $N = n_0 + n_1$ is the total number of particles in the beam, η is the number of gas molecules per cubic centimeter in the target gas, and x is the target distance traversed by the beam. With this relation (2.2) values for ϕ_0 and $(\sigma_{01} + \sigma_{10})$ can be obtained experimentally from measurements of $\frac{n_0}{N}$ with known gas target thicknesses.

Much data has been gathered for the loss and capture cross sections.[9] If we wish to design a source of focused neutral particles we could design around the experimental cross sections that are available. This data, however, would tell us only the charge state of the beam relative to the gas target thickness. To be able to completely describe the neutral beam we must also have data available that tells us how the beam scatters as a function of the gas target thickness. An example of such a problem will be given later in this work.

2.2 Scatter Theory

The collisions between two particles or a particle with a fixed force field can be broken up into two one particle problems. One describes the motion of the particles relative to each other or to their center of mass, and the other describes the free motion of the center of mass. Two coordinate systems can be used for calculations and measurements. The "laboratory system" has the bombarded particle initially at rest while the "center-of-mass system" has the center of mass of the system always at rest.

Particles in the two systems and the angular relations between them are shown in Figure 2.1. Both systems will be used as it is easier to calculate the result of a collision in the "center-of-mass system" while all experimental measurements are made with reference to the "laboratory system".

Let us suppose we have a parallel flux of N particles per unit area per unit time incident on a group of η particles or scattering centers, and count the number of emergent particles per unit time in a small solid angle $\Delta\omega_0$ centered about a direction that has polar angles θ_0 and ϕ_0 with respect to the incident axis. This number will be proportional to N, η, and $\Delta\omega_0$, provided that there is no interference between the incident particles and no appreciable loss of the incident particles by their recoil out of the target region. This number of particles can be written

$$\eta N \sigma_0(\theta_0, \phi_0) \Delta\omega_0 \tag{2.21}$$

where $\sigma_0(\theta_0, \phi_0)$ is a constant of proportionality and is called the differential scattering cross section. It has the dimensions of area.

The total scattering cross section is defined as the integral of $\sigma_0(\theta_0, \phi_0)$ over the sphere.

$$\sigma_0 = \int \sigma_0(\theta_0, \phi_0) d\omega_0 \tag{2.22}$$

For the collision of a particle with a fixed scattering center this definition is valid in both coordinate systems. However, for a collision between two particles of finite mass, it applies only to the laboratory system and the scattered incident particle. Relations

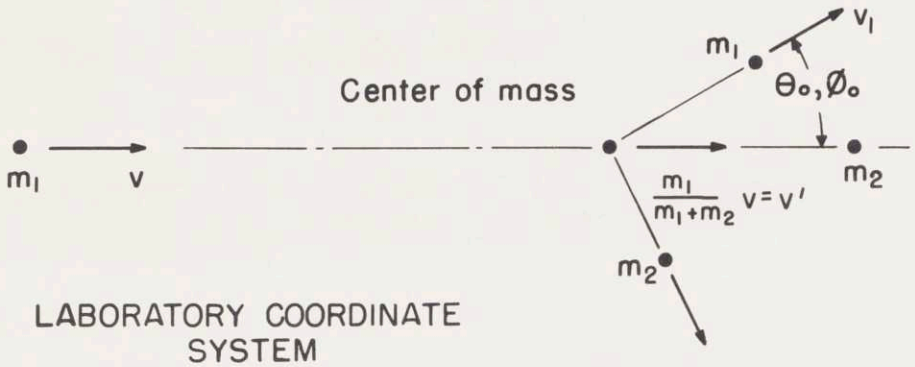

LABORATORY COORDINATE SYSTEM

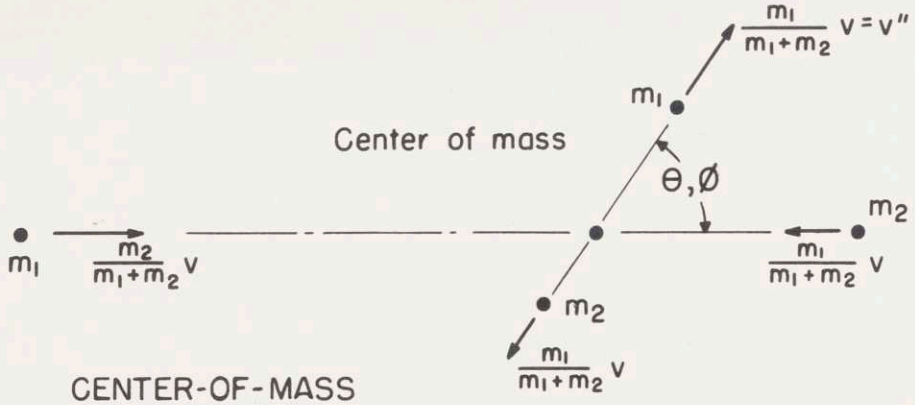

CENTER-OF-MASS COORDINATE SYSTEM

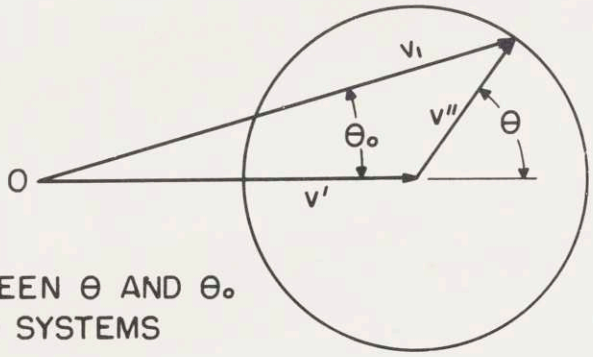

RELATION BETWEEN Θ AND Θ_o IN THE TWO SYSTEMS

Fig. 2.1

between the two can be obtained from Figure 2.1 to be

$$\sigma_0(\theta_0, \phi_0) = \frac{(1 + \gamma^2 + 2\gamma\cos\theta)^{3/2}}{(1 + \cos\theta)} \sigma(\theta, \phi) \qquad (2.23)$$

where $\gamma = \frac{m_1}{m_2}$. The total cross section is the same for both systems since the total number of collisions that take place is independent of the mode of description of the process.

It has been shown that the collision process according to wave mechanics is equivalent to the scattering of a plane wave of wave length $\lambda = \frac{h}{\mu v_r}$ by an opaque sphere of radius a where μ is the reduced mass $\mu = \frac{m_1 m_2}{m_1 + m_2}$, and v_r is the relative velocity of approach.[2] If we write the wave equation

$$-\frac{\hbar^2}{2\mu}\nabla^2 u + Vu = Eu \qquad (2.24)$$

we can think of it as representing the collision of a particle of mass μ, initial velocity v, and kinetic energy $E = \frac{1}{2}\mu v^2$, with a fixed scattering center that is described by the potential energy $V(r)$. Then r is the vector distance from the fictitious particle to the origin of the scattering potential.

The wave function u may be written as a function of the angles θ and ϕ (Figure 2.1) and the distance r between the particles. Schiff[11] finds that the scattering is determined by the asymptotic form of $u(r, \theta, \phi)$ in the region where $V = 0$.

$$u(r, \theta, \phi) \underset{r \to \infty}{\longrightarrow} A\left[e^{ikz} + \frac{1}{r} f(\theta, \phi) e^{ikr}\right] \qquad (2.25)$$

where $K = \frac{\mu v}{\hbar} = \frac{2\pi}{\lambda}$ is the magnitude of the propagation vector. The first term is an infinite plane wave moving along the axis. The second term represents a particle that is moving radially outward whose amplitude depends on θ and ϕ and is inversely proportional to r. This wave function satisfies the wave equation given previously. The differential scattering cross section then is found to be

$$\sigma(\theta, \phi) = |f(\theta, \phi)|^2 \tag{2.26}$$

If we solve the problem for scattering by a perfectly rigid sphere[2] for low energies where $\lambda >> a$, $\sigma(\theta)$ is the same (at all angles) as for classical theory, but with σ_0 four times the classical value. In our case for high energy, i.e. $\lambda << a$, the differential cross section varies considerably with θ. For similar hard spheres, $\sigma(\theta)$ oscillates about the classical value of $\frac{a^2}{4}$ when θ is greater than a critical angle

$$\theta_c = \frac{\lambda}{2a} \tag{2.27}$$

and rises rapidly to a value $\sigma(\theta) = \frac{\pi^2 r^4}{\lambda^2}$ when $\theta \to 0$. Dissimilar hard spheres give about the same distribution except there is little oscillitory movement about the classical value. These two results are pictured in Figure 2.2.

The case of rigid spheres will possibly give an approximation of the noble gases with their closed shells. It was introduced, however, only to give a physical feeling for the scatter process. It seems more probable that the actual scatter process is very nearly that of

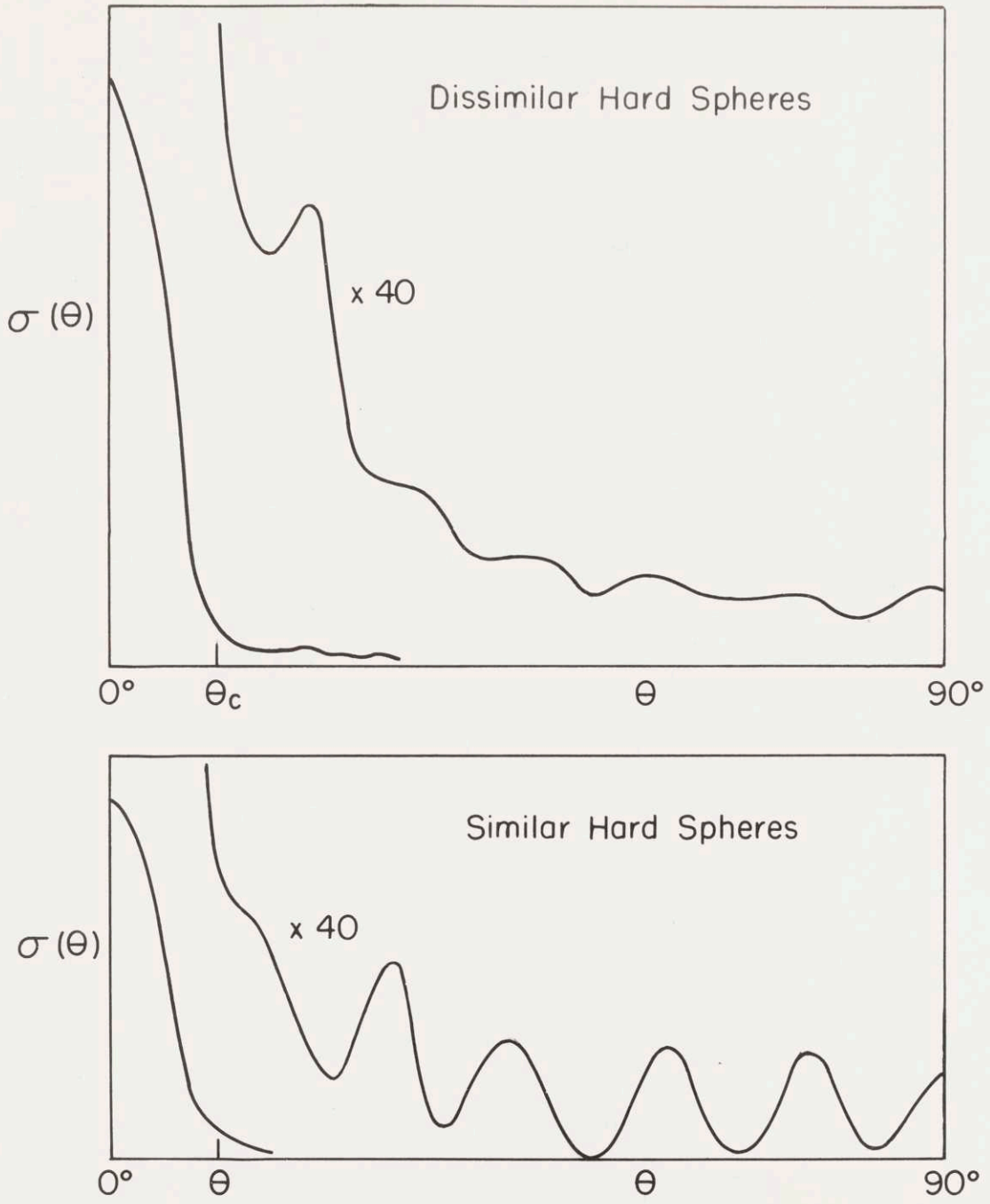

ANGULAR DISTRIBUTION PREDICTED BY WAVE THEORY

Fig. 2.2

a spherically symmetric square well potential. In the case of the He - He collision for example: van de Waals force is proportional to r^{-6} so beyond a certain distance there will be no forces acting between the two particles.

The case for the spherically square well potential is more difficult to solve than for rigid spheres, but for high energies, i.e. $Ka >> 1$ a method using the Born approximation can be used.[11] An approximate solution to the wave equation (2.24) is obtained

$$u(\bar{r}) = e^{iKz} - (4\pi)^{-1}\int |\bar{r}-\bar{r}'|^{-1} e^{iK|\bar{r}-\bar{r}'|} e^{iKz'} U(\bar{r}')\, d\tau' \qquad (2.28)$$

The second term (2.28) has the form of a superposition of waves scattered from all points $\bar{r}'$ with their amplitudes proportional to the product of the incident wave amplitude and the scattering potential at those points.

It is assumed that $U(\bar{r}')$ falls off fast enough for large r' so that there is an asymptotic region in which r is large in comparison with those values of r' which contribute significantally to the integrand.

Then $|\bar{r}-\bar{r}'| \underset{r\to\infty}{\longrightarrow} r - \alpha r'$; $|\bar{r}-\bar{r}'|^{-1} \underset{r\to\infty}{\longrightarrow} \frac{1}{r} + \frac{\alpha r'}{r^2}$

where α is the cosine of the angle between the vectors $\bar{r}$ and $\bar{r}'$. The asymptotic form of (2.28) then is

$$u(\bar{r}) \to e^{iKz} - (4\pi r)^{-1} e^{iKr}\int U(\bar{r}')\, e^{iK(z-\alpha r')}\, d\tau' \qquad (2.29)$$

and the scattered amplitude is

$$f(\theta,\phi) = -(4\pi)^{-1}\int U(\bar{r}')\, e^{iK(z'-\alpha r')}\, d\tau'$$

$$= -(4\pi)^{-1}\int U(\bar{r}')\, e^{i\bar{P}\cdot\bar{r}'}\, d\tau' \qquad (2.30)$$

where $\bar{P} = \bar{K}_0 - \bar{K}$. $\bar{K}_0$ is a vector of magnitude K in the direction of the incident beam axis. $\bar{K}$ is a vector of magnitude K in the direction of the polar angles (θ, ϕ) of the point at which the scattered amplitude is measured. $\bar{P}$ has a physical significance that $\hbar\bar{P}$ is the momentum transferred from the incident particle to the scattering potential during the collision.

If $U(\bar{r}) = U(r)$ is spherically symmetric, the integral over the polar angles or $\bar{r}'$ in (2.30) can be evaluated by taking the direction of $\bar{P}$ as the polar axis. Then

$$f(\theta) = -P^{-1}\int_0^\infty r' \sin Kr'\; U(r')\, dr' \qquad (2.31)$$

As one would suspect, the scattered amplitude is independent of the angle ϕ.

If we now apply the result (2.31) to the scattering of a square well potential we find

$$f(\theta) = \frac{2\mu V_0}{\hbar P^3}(\sin Pa - Pa\cos Pa)$$

where $P = 2K\sin\frac{\theta}{2}$. The differential scattering cross section is

$$\sigma(\theta) = \left(\frac{2\mu V_0 a^3}{\hbar}\right)^2 g(2Ka\sin\tfrac{\theta}{2}) \qquad (2.32)$$

with $g(x)$ defined as

$$g(x) \equiv \frac{(\sin x - x\cos x)^2}{x^6}$$

At the high energies we are interested in ($Ka >> 1$), most of the scattered particles are continued in a cone whose angular spread is of the order of $\frac{1}{Ka}$, where a is the radius of the scattering potential well. Then the critical angle is

$$\theta_c = \frac{1}{Ka} \tag{2.33}$$

which is less than the value obtained by assuming rigid spheres (2.27) by a factor of $\frac{1}{\pi}$. The validity of the Born approximation for high energy collisions ($Ka >> 1$) is verified by Schiff[12].

The apparatus is designed with an angular aperture of 0.017 radians presented to the beam as it enters the gas target. This means that a particle scattered more than this amount will not leave the target region in the beam.

The critical angle for a 20 kev helium atom colliding with an argon atom should give the maximum angle any particles will be scattered into. This angle will be calculated to verify that there is no limitation by the apparatus for the energy range in which we are interested.

$$K = \frac{\mu v_r}{\hbar} = 3.08 \times 10^{13}$$

If we take a as the radius of the outer shell of argon $a = 6.7 \times 10^{-11}$ meters.

$$\theta_c = \frac{1}{Ka} = 4.85 \times 10^{-4} \text{ radians}$$

which is almost two orders of magnitude smaller than the apparatus limitation. This critical angle is for only one collision per incident particle but any additional collisions will take place further

along in the target tube and the angular aperture will be effectively increased so that there will not be any limitation by the apparatus in the range of measurements we are making.

These past discussions have all been for particles undergoing a single collision. This is not the case in this experiment. Using measured charge transfer cross sections, the average number of collisions can be calculated to be from 1 to 10 for the gas target thickness range used. Bothe[14] described scattering by small numbers of collisions as plural scattering and indicated that it could be described by a Gaussian error curve expressed in two dimensions. For small angles i.e. $\theta \approx \sin\theta$

$$N\,d\Omega = N_0 \frac{d\Omega}{2\pi\lambda^2} e^{-\frac{\theta^2}{2\lambda^2}} \qquad (2.34)$$

where

N_0 is the number of incident particles

$N\,d\Omega$ is the number of particles scattered into the elemental sold angle $d\Omega$.

λ is the most probable deflection, i.e. the value of θ for which $N\theta$ is maximum.

ϕ is the cone angle which contains half of the scattering, as pictured in Figure 2.3.

If we let $\int_0^{\phi} N\,d\Omega = \frac{N_0}{2}$ and write $d\Omega$ as $2\pi\theta\,d\theta$ then (2.34) is

$$-\int_0^{\phi} e^{-\frac{\theta^2}{2\lambda^2}}\left(-\frac{\theta}{\lambda^2}\,d\theta\right) = \frac{1}{2}$$

$$1 - e^{-\frac{\phi^2}{2\lambda^2}} = \frac{1}{2}$$

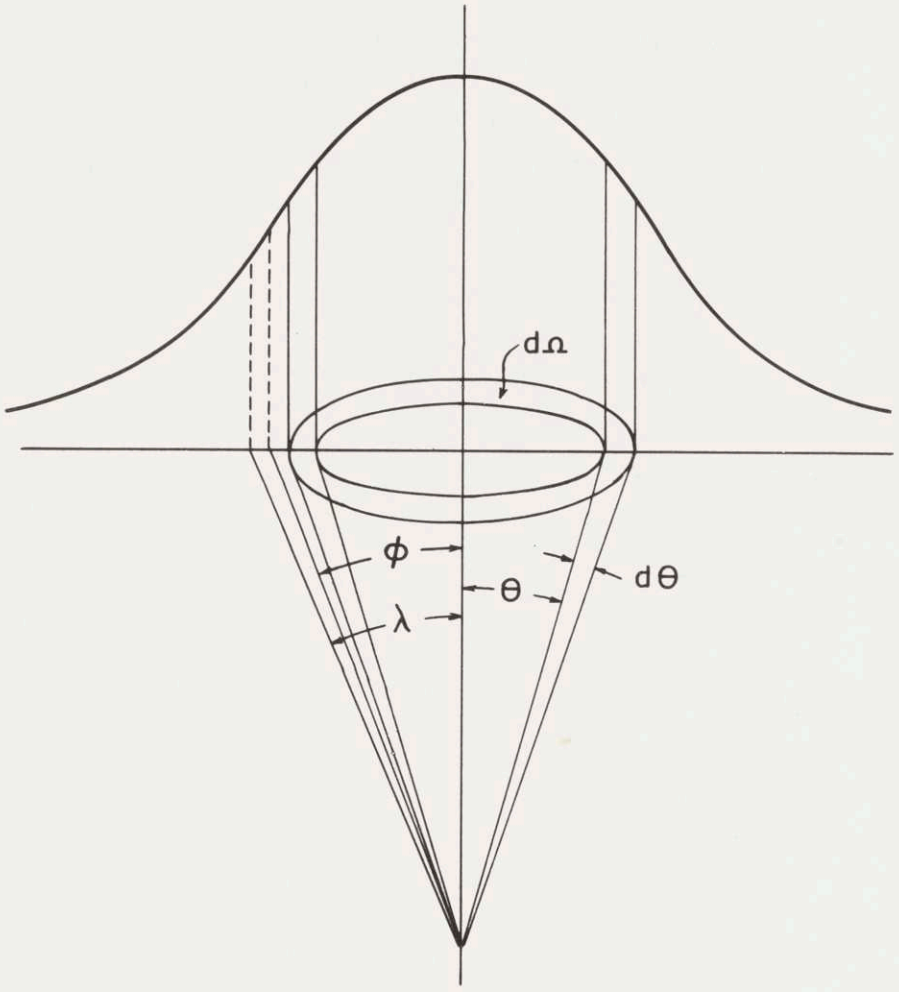

TWO DIMENTIONAL GAUSSIAN DISTRIBUTION

Fig. 2.3

$$\phi = \lambda \sqrt{2 \ln 2} = 1.18 \lambda \qquad (2.35)$$

The most probable deflection should be a function of incident particle mass, target particle mass, incident particle energy, and gas target thickness.

$$\lambda = f(m_1, m_2, E, T) \qquad (2.36)$$

An attempt will be made to find an empirical ϕ from the experimental data in Chapter IV. Also the measured ϕ will be compared with a computed θ_c at very thin targets where single collision scattering is probable to see if any correlation can be made between them.

CHAPTER III

EXPERIMENTAL WORK

3.1 Description of Apparatus

The apparatus used, pictured in Figure 3.1, is a modification of that used by Philp[13] for his charge transfer measurements. It consists of an ion source and associated beam forming and accelerating equipment, a charge transfer region, a magnetic analyzing system, and a drift tube with facilities for measuring the neutral beam dispersion.

P_1, P_2, P_3, and P_4 are high speed oil diffusion pumps that maintain the vacuum throughout the system with the aid of differential pumping constrictions. The constriction in E_2 permits differential pumping of the gas that enters the system from the ion source. D_1 and D_2 do the same for the gas from the charge transfer region.

Individual parts of the total system will be explained in greater detail below.

3.11 Ion Beam Forming Apparatus

The positive ions are formed by a r-f source, I, produced by the High Voltage Engineering Corporation. Any type of gas can be introduced through a needle valve which controls the flow and therefore the pressure in the plasma. The frequency used was between 120-125 mc. Pressure and frequency were adjusted to give optimum performance for the particular gas used.

The accelerating and focusing section A is formed of glass rings fastened together with a thermoplastic vinyl-acetate polymer. A high

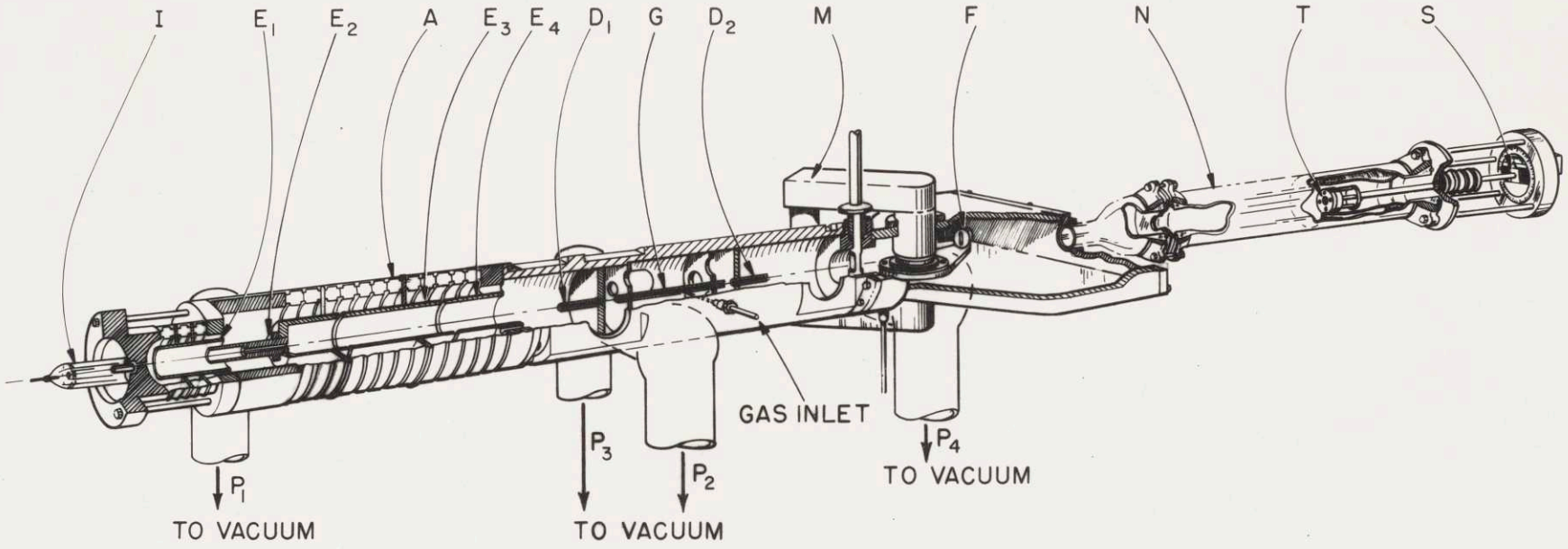

HIGH ENERGY NEUTRAL BEAM APPARATUS

Fig. 3.1

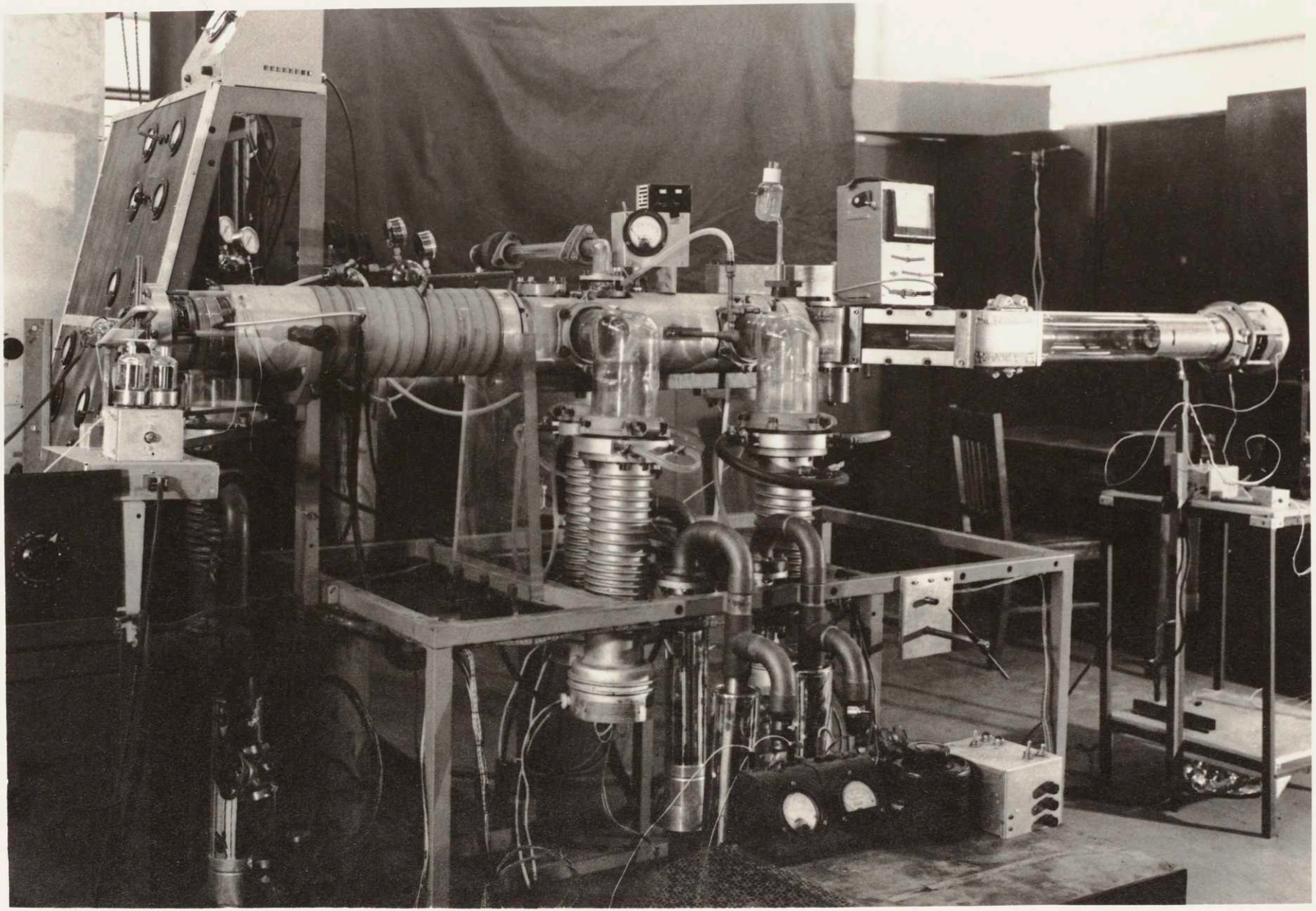

Fig. 3.2

vacuum of approximately 10^{-5} mm Hg is maintained in this region.

E_1 and E_2 are the beam forming electrodes. They are connected to a 0-20 kv power supply through a voltage divider network that allows a wide range of potential combinations of which the optimum is selected experimentally. E_3 and E_4 are the accelerating electrodes and are connected through voltage dividing resistors to a 0-80 kv power supply. By a proper combination of voltage dividing resistors and power supply potentials, a well focused ion beam of variable energy is obtainable. The beam, however, is unstable at energies above 45 kev due to corona from the large metal area of the apparatus which is kept at the accelerating potential.

A 1 mm defining hole is placed at the end of D_1 to insure a small beam of uniform cross section incident upon the gas target.

3.12 Charge Transfer Region

The charge transfer region consists of a gas filled tube 5 mm diameter and 20 cm long with a provision for controlling gas flow into its center. This then controls the pressure in the tube. This pressure is measured at the center of the tube with a thermocouple gauge. The gas target thickness is the average pressure multiplied by the tube length. It is measured in units of micron-cm. The factor for converting the target thickness from micron-cm to atoms per cm^2 is 3.56×10^{13} atoms per cm^3 per micron.

The average pressure calculations were taken from previous data[13]. These calculations were made on a theoretical basis and a hot wire temperature loss experimental method. The curves obtained as a result of

each of these methods are shown in Figure 3.3.

The thermocouple gauge used for measuring the gas target thickness was originally calibrated for hydrogen. The readings must therefore be corrected when other gases are used in the target tube. To find a correction coefficient we must consider the heat loss equation for a thermocouple gauge.(16)

$$E = \alpha \Lambda P \sqrt{\frac{273.2}{T_s}} \quad (T_f - T_s) \tag{3.1}$$

E is the energy transfer per unit area from the filament to the outside shell.

α is the accomodation coefficient.

Λ is the free-molecule heat conductivity.

P is the pressure.

T_f is the filament temperature.

T_s is the shell temperature.

Then the ratio of the pressure of any gas x, to that of hydrogen at the same thermocouple gauge reading is

$$C_x = \frac{P_x}{P_{H_2}} = \frac{(\alpha \Lambda)_{H_2}}{(\alpha \Lambda)_x} \tag{3.2}$$

By using recorded values for the free-molecule heat conductivity(16) and accomodation coefficients(17) and equation (3.2) we can obtain pressure correction coefficients for the gases used. These coefficients are listed in the table below.

Gas	Coefficient
H_2	1
He	1.02
Ne	1.16
A	1.64

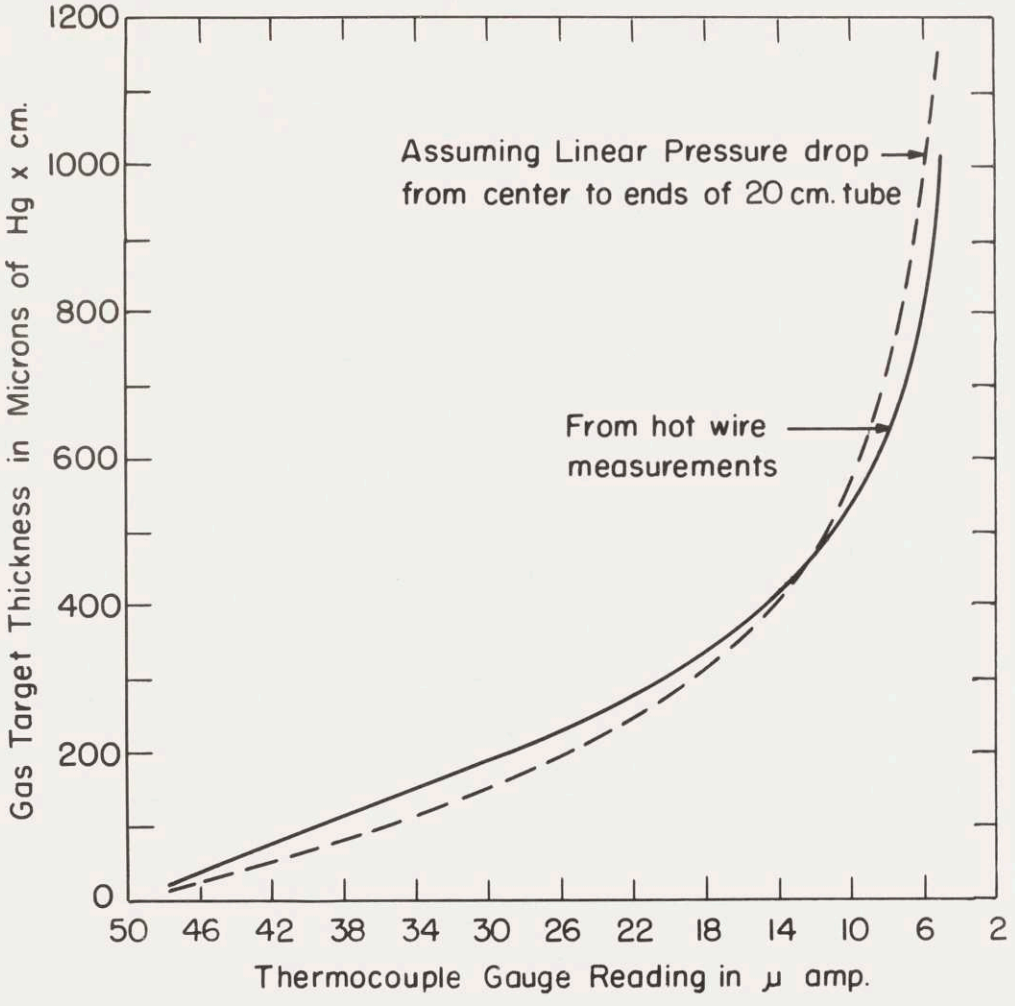

Fig. 3.3 GAS TARGET THICKNESS AS A FUNCTION OF THERMOCOUPLE GAUGE READING

3.13 Magnetic Analyzer and Ion Measuring

M is the analyzing magnet used to sweep the charged component from the mixed beam. Six 1 x 1 x 6 inch alnico bars which have been saturated by a magnetization of 50,000 oersted form the permanent magnet whose poles protrude through the top and bottom of the analyzing chamber and meet in a 1/4 inch gap. The field in this gap can be varied by changing the air gap in an external magnetic shunt.

A Faraday cage is mounted on an arm which pivots about the magnetic pole piece. This arm can be moved $\pm$ 50 degrees from the center axis of the neutral beam. The current received in the Faraday cage is measured by a Ultra-Sensitive R.C.A. microammeter. The Faraday cage was used to measure the total ion beam current in the secondary electron emission data and to determine the positive ion content of the incident ion beam. The neutral beam measurements were made at the end of the drift tube.

3.14 Measurement of Neutrals

The drift tube N has two purposes. First, it provides a long distance for the neutral beam to travel after the collisions in the gas target. This permits the dispersion of the beam to become great enough for the cross section to be easily measured. Second, it allows the beam to drift to ground potential so all the measuring and recording equipment is not required to be kept at the accelerating potential.

3.141 Target Construction

There are three general methods for measuring neutral beam

current. The ionization method used by Meyer and by Wayland[19] in which the beam causes ionization in a chamber and this ionization current is measured. The thermal method in which the intensity of the beam is determined by the heating effect it produces when striking a thermal element. This method was used by Amdur and Pearlman[18]. The secondary electron emission method in which the beam strikes a metal surface and the electron current is collected and measured on a positive electrode. A target for this method is very simple to construct and as we had sufficient beam current and meter sensitivity for easy detection, a secondary electron emission type of target was chosen.

In section 2.2 we have deduced that the scattered particle distribution can be described by a Gaussian error curve given in equation (2.34). If we then consider the particle density distribution for a given gas target thickness as the volume of a solid Gaussian distribution, we can calculate the volume and thereby the particle density as a function of r. Cylindrical coordinates are best suited for this calculation and the differential volume from Figure 3.4 is

$$dV = 2\pi z r \, d\theta \, dr = 2\pi e^{-\frac{r^2}{2}} r \, d\theta \, dr$$

$$V = 2\pi \int_0^R \int_0^{2\pi} e^{-\frac{r^2}{2}} r \, d\theta \, dr$$

$$V = 4\pi^2 \left(1 - e^{-\frac{R^2}{2}}\right)$$

If we normalize this volume then

$$V = 1 - e^{-\frac{R^2}{2}}$$

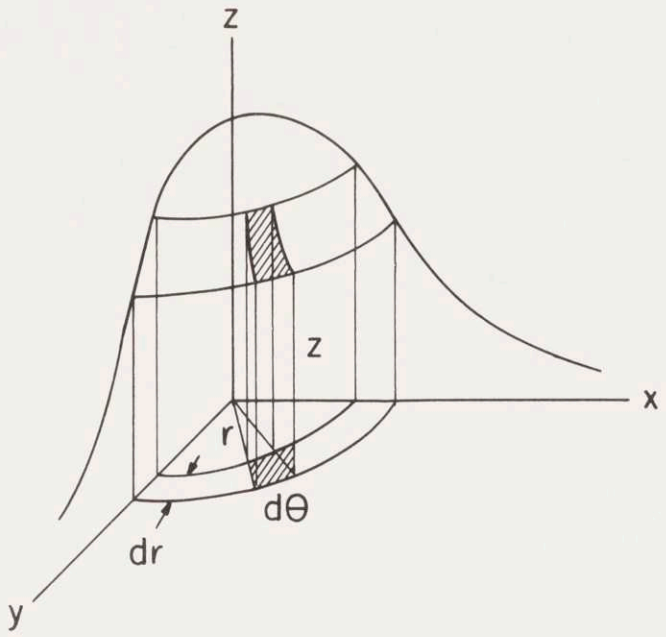

SOLID GAUSSIAN DISTRIBUTION

Fig. 3.4

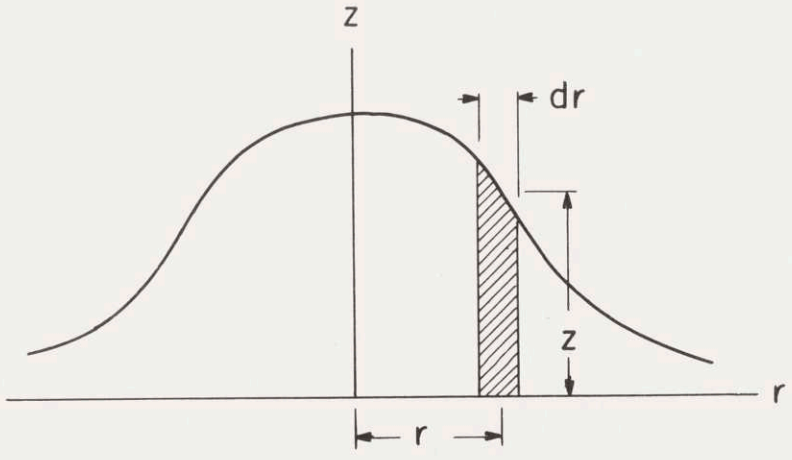

TWO DIMENSIONAL GAUSSIAN DISTRIBUTION

Fig. 3.5

is the percentage of the total particles that lie in a cylinder of radius R.

Now designate B_0 as the value of R for which V = 1/2. Then

$$\frac{1}{2} = 1 - e^{-\frac{B_0^2}{2}}$$

$$e^{-\frac{B_0^2}{2}} = \frac{1}{2}$$

$$B_0^2 = 2 \ln 2$$

$$B_0 = \sqrt{2 \ln 2} = 1.18 \qquad (3.3)$$

Figure 3.5 gives a two-dimensional plot of the particle density. Here $z = e^{-\frac{r^2}{2}}$. If we normalize the curve by letting $z = 1$ when $r = 0$ and find the value of r when $z = \frac{1}{2}$ we find

$$\frac{1}{2} = e^{-\frac{r^2}{2}}$$

$$r = 1.18 \qquad (3.4)$$

This is the value of r for the half-width of the curve and is the same value as found for the half-volume of the solid distribution (3.3).

This indicates that one method of measuring the particle distribution would be to obtain the half-width of the two-dimensional distribution. This can be done by sweeping a small opening along a beam cross-sectional diameter and plotting the number of particles passing through this opening as a function of r. This will give a two-dimensional plot if the opening is small in relation to the beam width. From calculations based on the results of Chapter II it appears that we will have beams with widths of the order of 1 mm. The sensitivity of the measuring equipment is such that an opening of less than 1 mm would not be feasible.

A target, shown in Figure 3.6, was constructed with d equal to 1 mm diameter. I is an insulator and T_1 is kept at 45 volts positive with respect to T_2. Thus any secondary electrons the neutrals may cause to be emitted from T_2 are collected on T_1. This current is amplified and sent to an Esterline-Angus pen recorder.

The whole target assembly is on an arm that passes through a vacuum seal and is connected to a motor driven sweep drive. The target moves across the beam at a rate of 0.93 mm per second. The pen recorder chart speed is 5.1 mm per second. These combinations of target and chart speed give very good results. It is not necessary to consider the secondary electron emission coefficient as by taking the half-width we effectively normalize the height.

The half-width that we measure directly from the chart is not the true half-width in equation (3.3). We will designate this measured half-width as B_M. The chief difference between the two is the fact that B_M is measured with an opening of finite size whereas B_o assumes a vanishingly small opening. We must therefore derive a correction formula for measuring with a finite opening.

Consider the distribution cross-section on a polar graph shown in Figure 3.7. Draw in an arbitrary B_o and compute the volume included by a cylinder of diameter d at several ψ values. Three values of d are used; $d = B_o$, $d = B_o/2$, and $d = B_o/4$. This volume was calculated by mechanical integration for ψ points of 0, B_o, $2B_o$, and $3\ B_o$.

The mechanical integration was done by using differential shells of 0.1 ψ units and 10^o angular increments. A table of calculated error

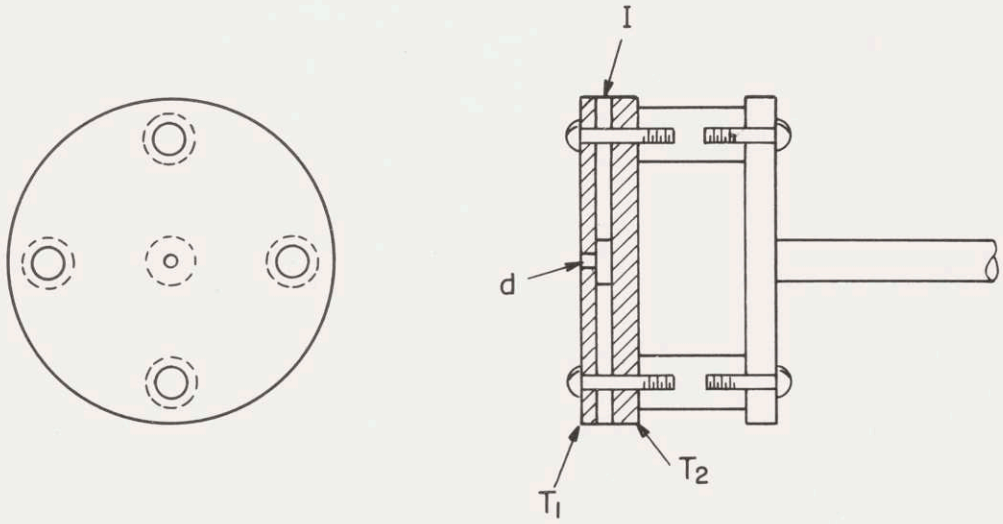

BRASS TARGET
FOR NEUTRAL BEAM

Fig. 3.6

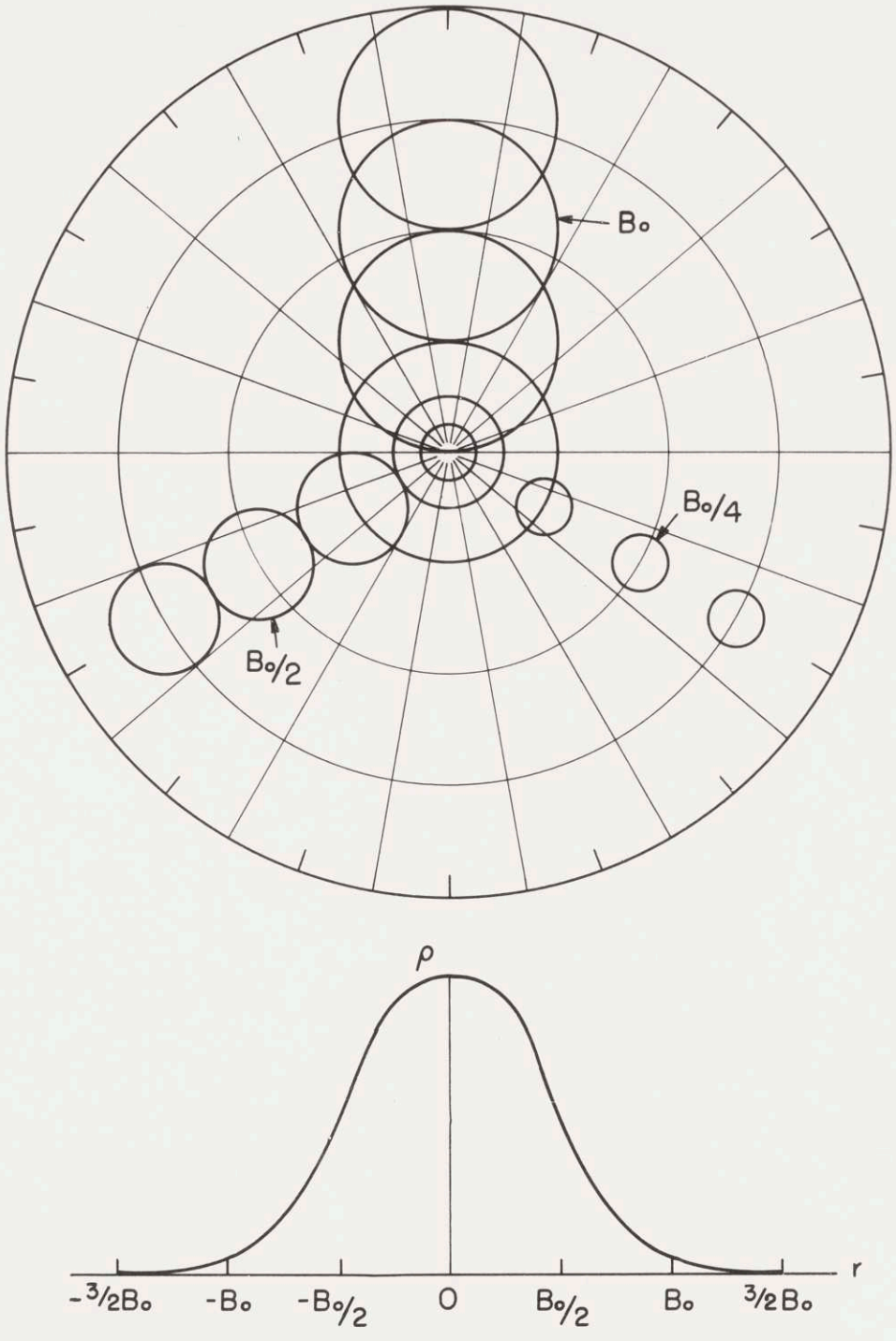

DIFFERENT VALUES OF d ON A POLAR DISTRIBUTION

Fig. 3.7

function values was used.[20] This calculated volume (with the total volume normalized) should be equal to the normalized current that would be measured through an opening of the same relative size in the particle beam.

The results from these calculations are plotted, holding d constant and letting B_o vary. In Figure 3.8 these plots are shown with current plotted against B_o/d. Also a plot of the true Gaussian curve is given which should be a plot of the current for $d = 0$. The half-widths of these curves are designated as B_M, the measured half-width. In all cases $B_M > B_o$ except for $d = 0$ where $B_M = B_o$.

Let us now consider a graph where we plot B_o/d. If $B_M = B_o$ we would have a diagonal line at 45^o. This, however, is not the case except for a vanishingly small opening. If we plot the three points we have calculated, the curve shown in Figure 3.9 is obtained. The curve can be extended by considering the half-width that would be measured for an infinitely small beam with an opening d. We find $B_M/d = 1$. We can then extend the curve (dotted portion) to the point (1, 0). We are uncertain of the exact shape of the curve in this region so it is preferable not to use this method when $B_o < d$.

For a very close approximation of the correct B_o from B_M we can use the following formula obtained from Figure 3.9.

$$B_o = B_M - 0.2\,d \tag{3.5}$$

We can now define a relative or percentage error as

$$E_r = \frac{0.2\,d}{B_o} \tag{3.6}$$

In Figure 3.10 E_r is plotted as a function of $\log\left(\frac{d}{B_o}\right)$ and shows

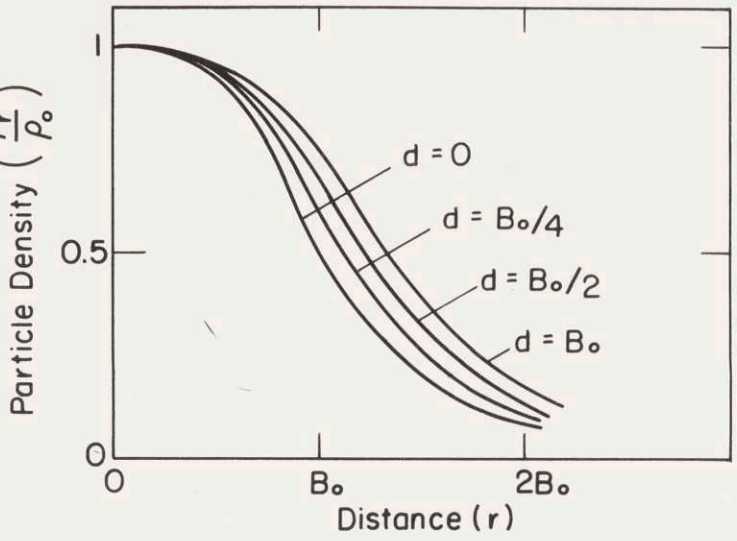

PLOT OF VARIABLE d RESULTS

Fig. 3.8

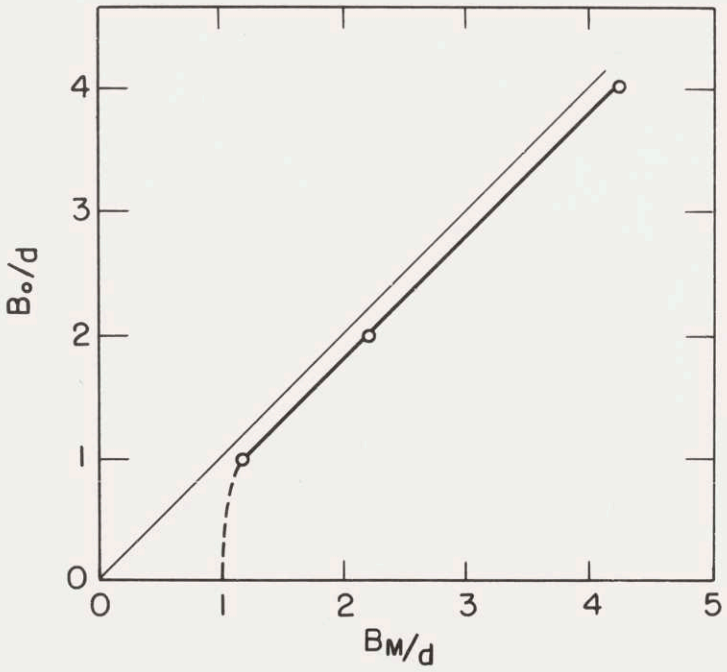

ERROR FROM VARIABLE d

Fig. 3.9

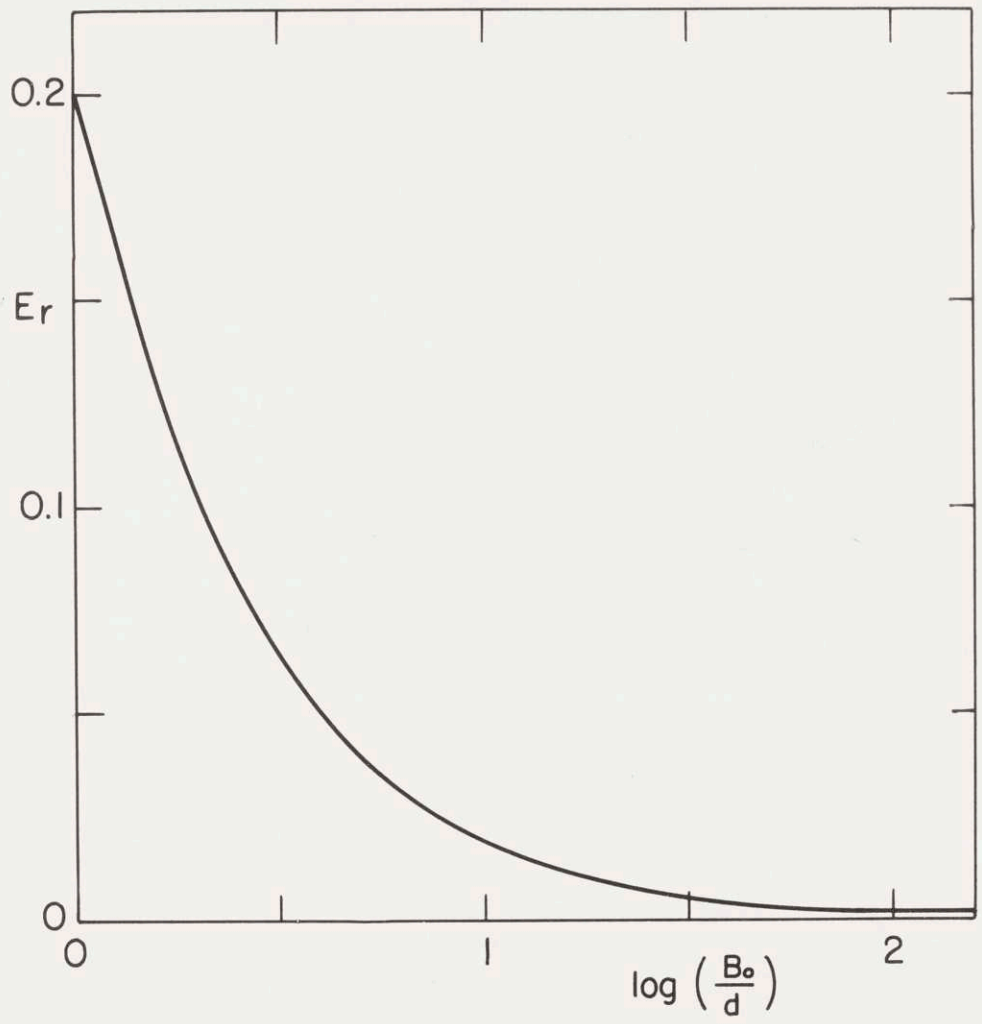

PERCENTAGE ERROR

Fig. 3.10

quite clearly that as d approaches zero the error goes to zero. Also in the range where we are working ($1 < \frac{B_o}{d} < 10$) the relative error is between 20 and 2 percent.

A second method for measuring B_o has been devised which also uses the Gaussian properties of the distribution.

We have assumed that the current passing through a hole is proportional to the volume of the Gaussian distribution included in a cylinder of the same diameter. If we make the axis of the cylinder and the axis of the distribution coincide, holding the distribution constant and varying cylinder, we can obtain data to plot the ratio of the volume or current in the cylinder to the total volume or current against B_o/d. This plot is shown in Figure 3.11. In the actual taking of data we can measure the current passing through the opening centered in the beam and find a value of B_o/d with the ratio I_d/I_r from the curve. As we know the value of d we can obtain B_o very easily. This method is useful only for $0.4 < B_o < 2.5$ d where the curve is changing rapidly.

Half-widths were measured using both methods and the results agreed within 3 percent.

Throughout this experiment the first method was used for the most part because it seemed a little easier to apply.

3.142 Effect of Focus Conditions

The focal length of the ion optical system plays a very important role in the amount of scatter present in the neutral beam. We are concerned with the amount of scatter the neutral beam has at a

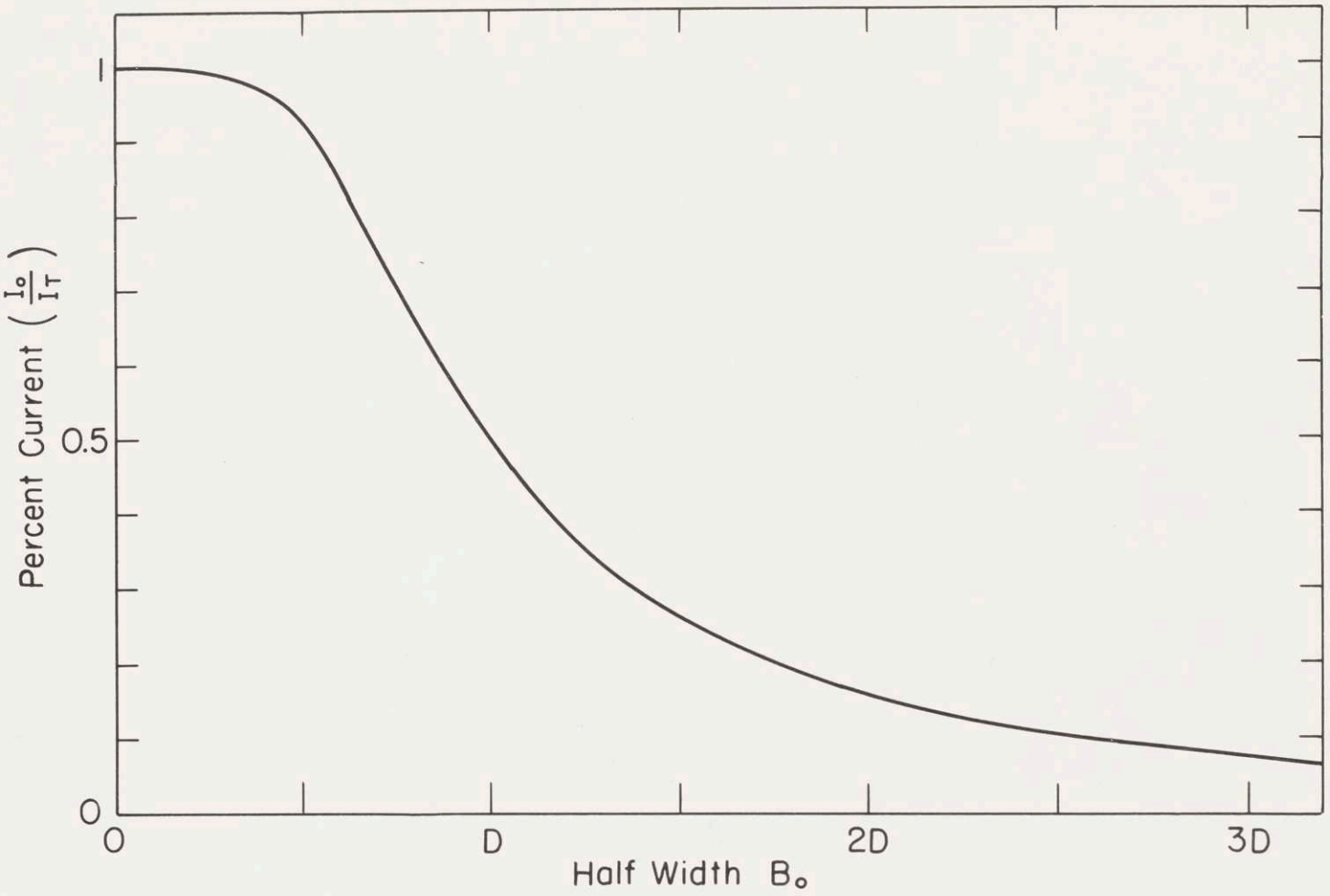

Fig. 3.11 CALCULATED FROM ASSUMED GAUSSIAN DISTRIBUTION

distance L from the charge transfer point.

Let us consider an ion beam that may be focused to a point anywhere along the axis of the system (neglecting the coulomb repulsive forces). The neutral beam formed from this ion beam will then be contained in a circle whose diameter is the ion beam diameter at that point, plus $2\lambda L$ where λ is the scattering angle and assumed to be small.

If we plot the ion beam diameter at L (Figure 3.12) as a function of focal length F (the distance from the gas target to the spot where the beam comes to a point) we obtain the curve shown in Figure 3.12 which obeys the equations

$$\frac{B}{\omega} = \frac{L - F}{F} \qquad 0 \leq \frac{F}{L} \leq 1 \qquad (3.7\ a)$$

$$\frac{B}{\omega} = \frac{F - L}{F} \qquad 1 \leq \frac{F}{L} < \infty \qquad (3.7\ b)$$

B is the diameter of a circle containing the total neutral beam

ω is the diameter of the ion beam incident on the transfer target

F is the focal length along the axis

L is the distance to the target

The above equations are for the case in which the scatter angle is zero. When there is a finite scatter angle λ, a constant must be added to the above equations giving

$$\frac{B}{\omega} = \frac{L + 2\lambda L F - F}{F} \qquad 0 \leq \frac{F}{L} \leq 1 \qquad (3.8\ a)$$

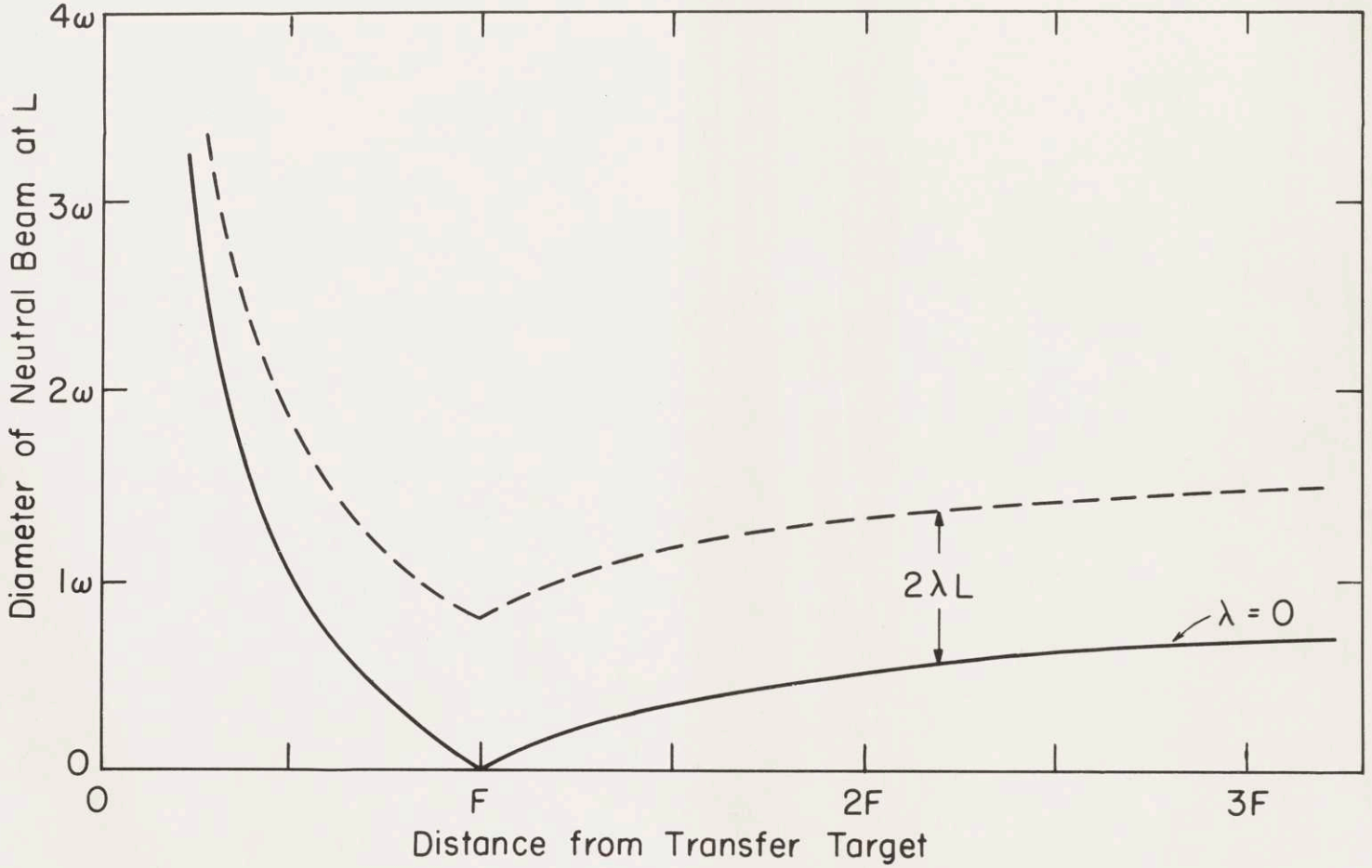

Fig. 3.12 EFFECT OF CHANGING FOCUS CONDITIONS

$$\frac{B}{\omega} = \frac{F + 2\lambda L F - L}{F} \qquad 1 \leq \frac{F}{L} < \infty \qquad (3.8\ b)$$

This does not change the shape of the curve but shifts it up a distance $2\lambda L$ as shown in Figure 3.12. It is easily seen that the smallest neutral beam at a distance L from the transfer target for any scattering angle will occur when $\frac{F}{L} = 1$, i.e., the focal length of the ion optical system is exactly the distance L. It must be remembered that an ion beam can never be focused to a point but this development is still applicable and shows the importance of correct focus conditions.

3.2 Scatter Measurement

The measurements were taken and the resulting curves are given in three parts grouped under the incident particles used: helium, neon, and argon. In each group the incident particle is scattered in a gas target of hydrogen, helium, neon, and argon. The same general procedure was used in all cases and will be described below.

The vacuum pumps are turned on for a sufficient length of time to allow the pressure of the system to reach approximately 10^{-5} mm Hg. Then the gases to be used are allowed to leak into the source and target area for 20 minutes to assure the purity of the source and target gases. The r-f oscillator is next turned on and a plasma formed by suddenly varying the gas pressure inside the source or by suddenly changing the inductive coupling. After the plasma is formed it is adjusted (pressure and r-f frequency) to a somewhat medium brightness glow.

The focusing and accelerating potentials are next applied along with the source probe voltage. The purpose of this source probe (which can be seen in the end of the pyrex source bottle in Figure 2.1) is to remove the excess electrons from the ionized plasma. The accelerating potential is set for the particle energy desired (20 to 40 kev in 5 kev steps in this experiment) and the three other variables; focusing potential, source probe voltage, and source pressure are adjusted for a maximum ion beam in the Faraday cage. Then a small amount of gas is let into the gas target, approximately 40 micron-cm, and the three variables are again adjusted for a maximum neutral beam with the target centered in the beam. The beam cross section is then recorded for different target thicknesses from 40 - 400 micron-cm. This same procedure is followed for different energies and target and source gases.

There is no provision for measuring the source pressure but it is believed to be greater than 10^{-3} mm Hg. A check on the purity of the ion beam showed over 95 percent of the beam to be singly charged positive ions of the gas used.

It will be shown how the curves for the He-Ne interactions were obtained as an example for all curves. Figure 3.13 shows a plot of the half-width after correction for the finite target opening with equation (3.5). Due to coulomb repulsive forces before neutralization and imperfections in the ion optical system, the half-width did not approach zero as the gas target thickness approached zero. The half-width curves extended to zero target thickness should show the

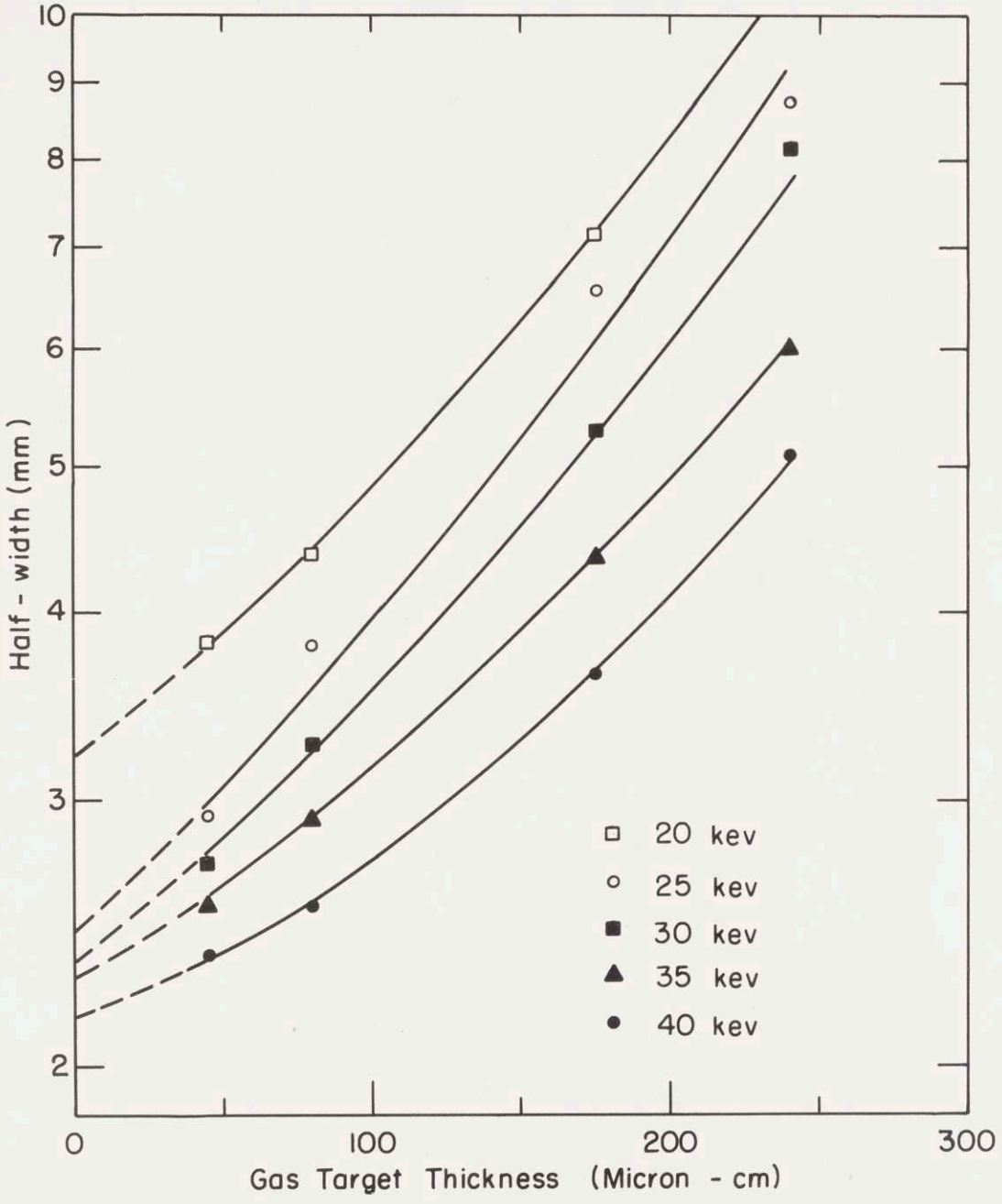

Fig. 3.13 HELIUM - NEON (Raw Data)

size of this spot which is inherently present and part of each curve. This constant value is then substracted from the data and a new plot made which should be the actual scattering half-width of the beam.

These curves are shown for helium incident particles in Figures 3.14 - 3.17, for neon incident particles in Figures 3.18 - 3.21, and for argon incident particles in Figures 3.22 - 3.25.

An attempt will be made to fit this data to curves and find the empirical relations between target thickness, scattering particle mass, and incident particle mass and energy in Chapter IV.

3.3 Secondary Electron Emission

Although the secondary electron emission data was not needed because of the normalizing of currents, data was taken for the three incident gases over the energy range used. The target plates T_1 and T_2 were shorted together and made positive with respect to the shielding cylinder. This made it possible to read the total neutral beam secondary electron emission current.

The Faraday cage was centered about the ion beam with zero gas target thickness; then a very thin gas target (20 micron-cm) was introduced and the neutral and ion currents noted. The gas target thickness was then increased to 50 micron-cm and the change in both ion and neutral currents noted. The ratio of the change in neutral current to the change in ion current is the secondary electron emission coefficient. The gas target thicknesses were kept thin so scatter would be negligible. The coefficients obtained for helium, neon, and argon are plotted against incident particle energy in Figure 3.26.

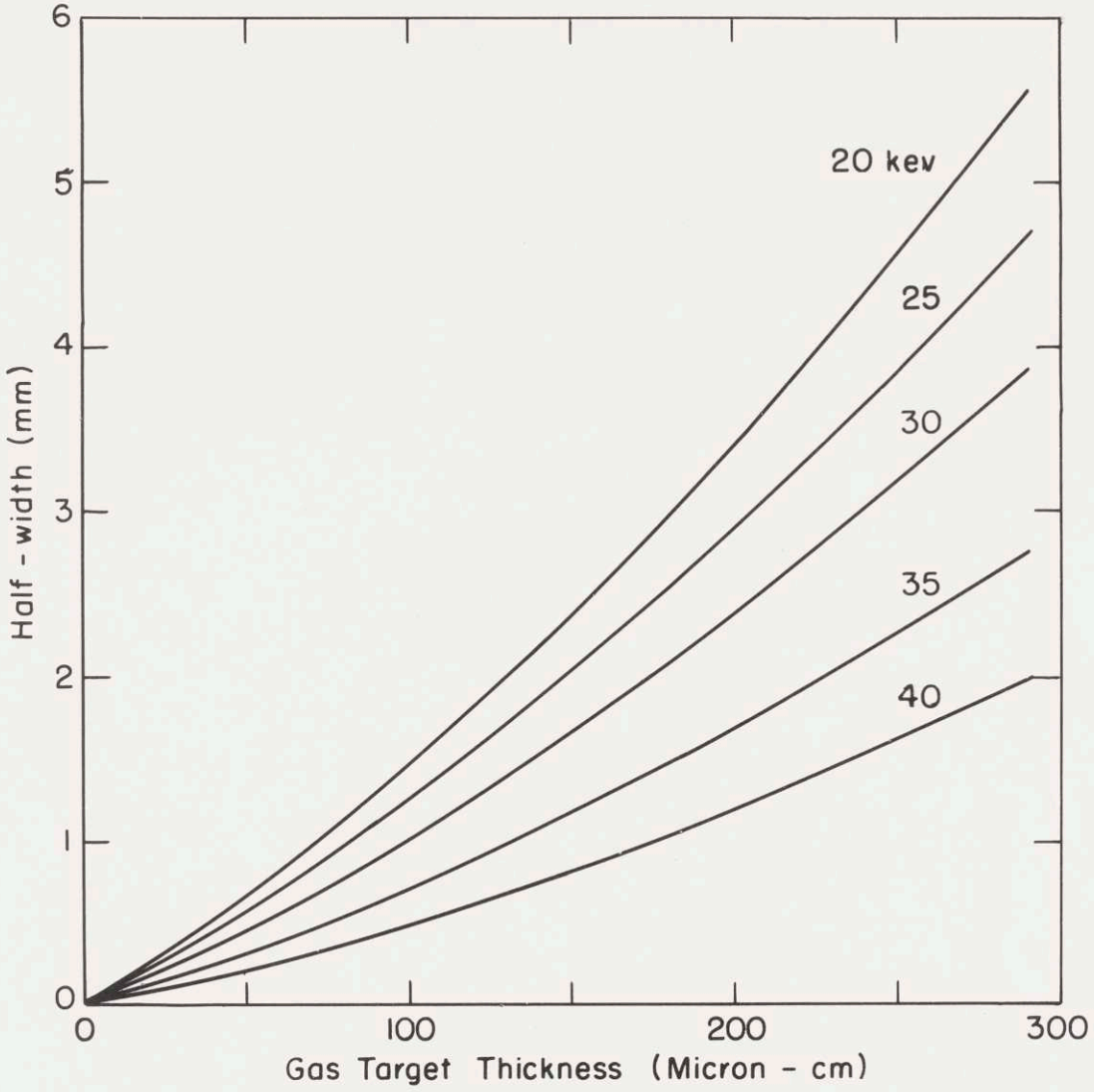

Fig. 3.14 HELIUM - HYDROGEN

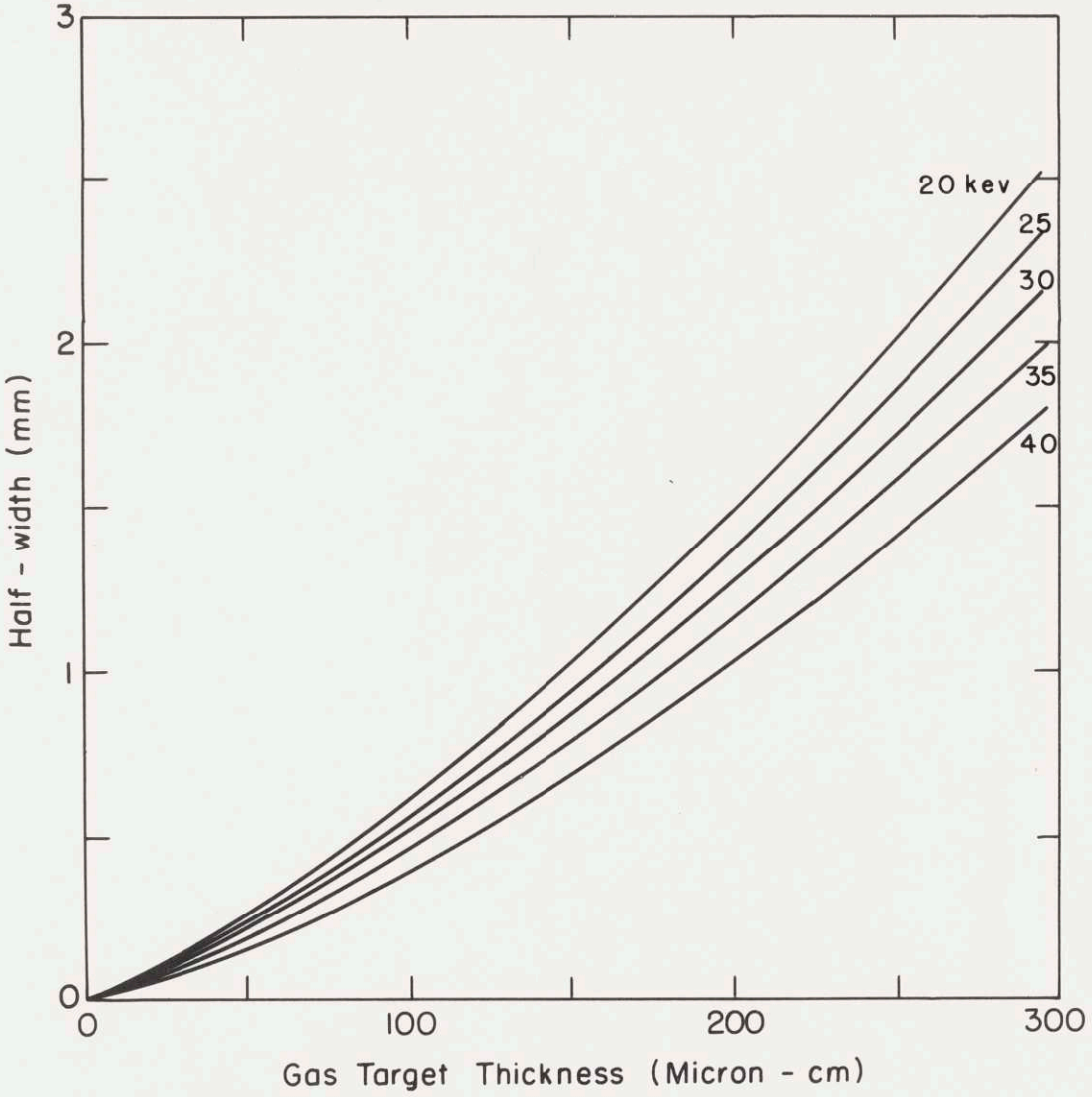

Fig. 3.15 HELIUM - HELIUM

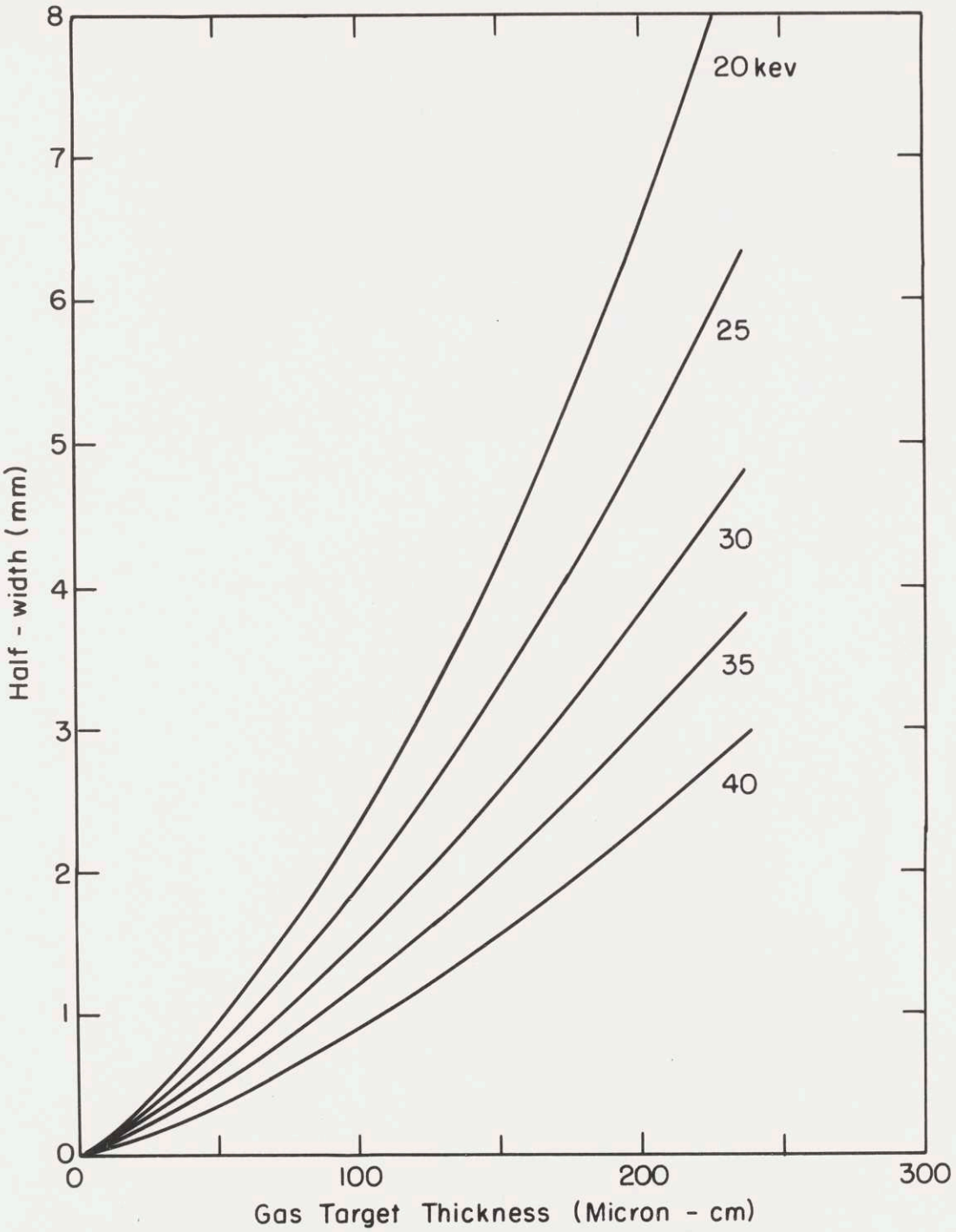

Fig. 3.16 HELIUM - NEON

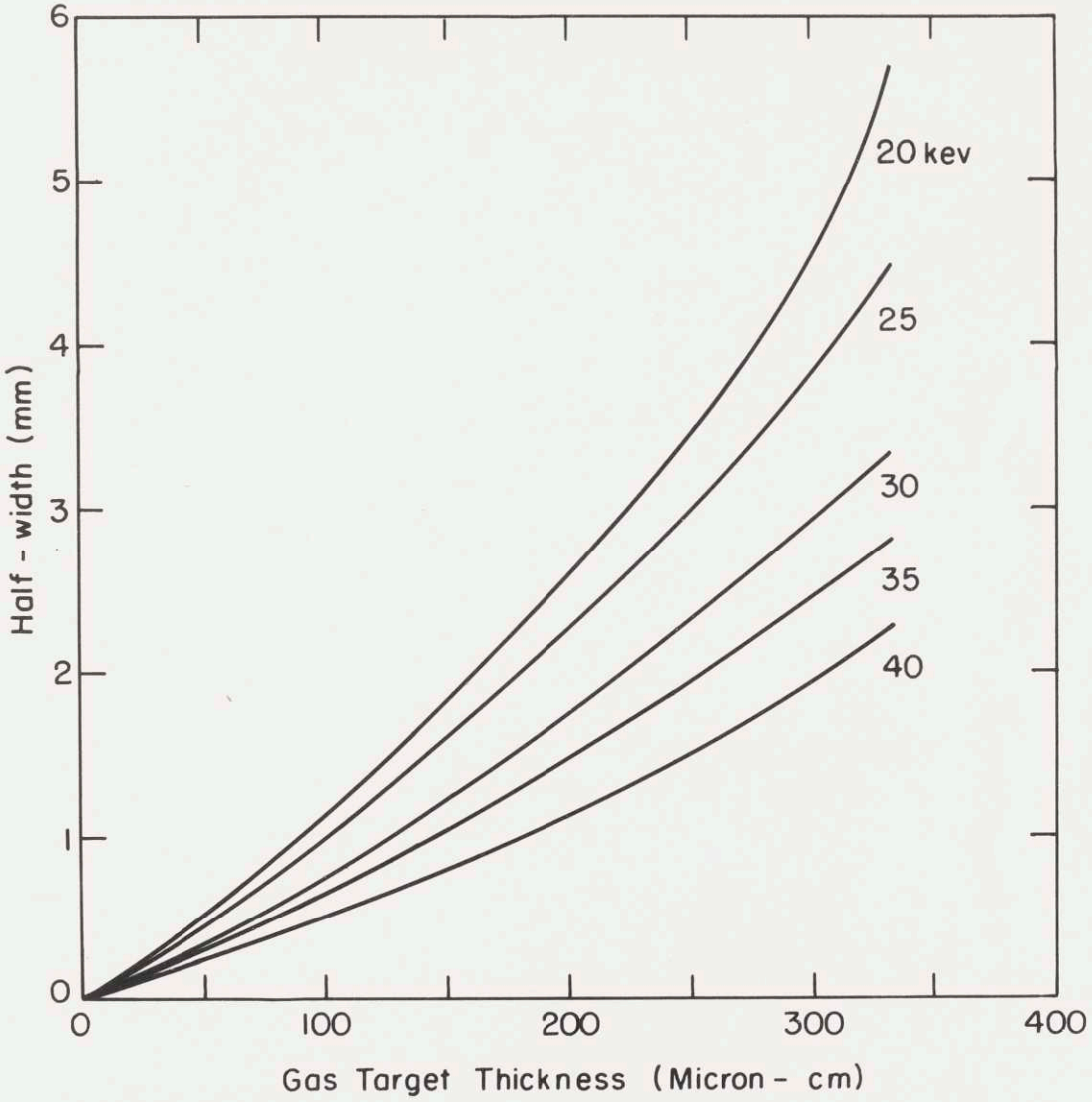

Fig. 3.17 HELIUM - ARGON

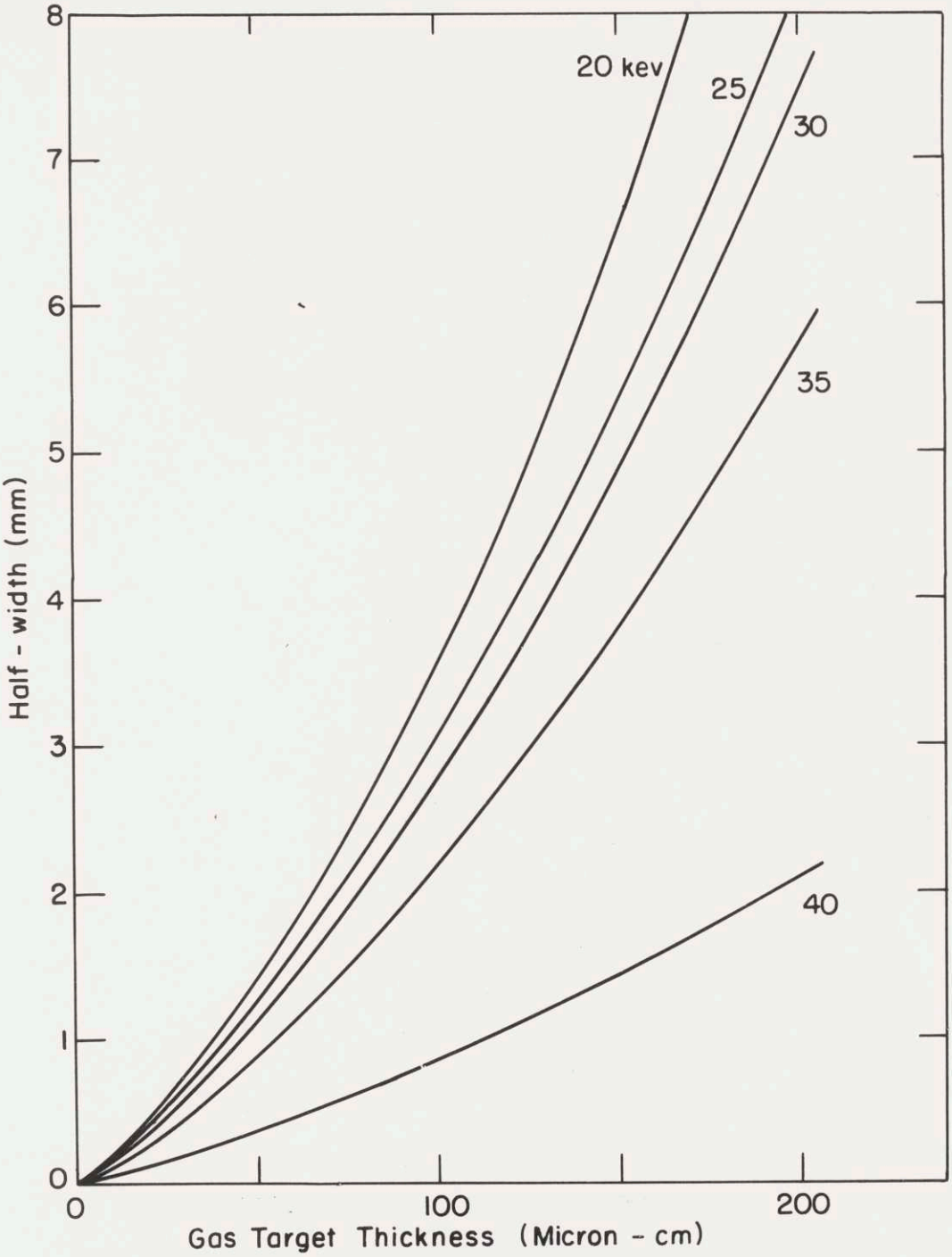

Fig. 3.18 NEON - HYDROGEN

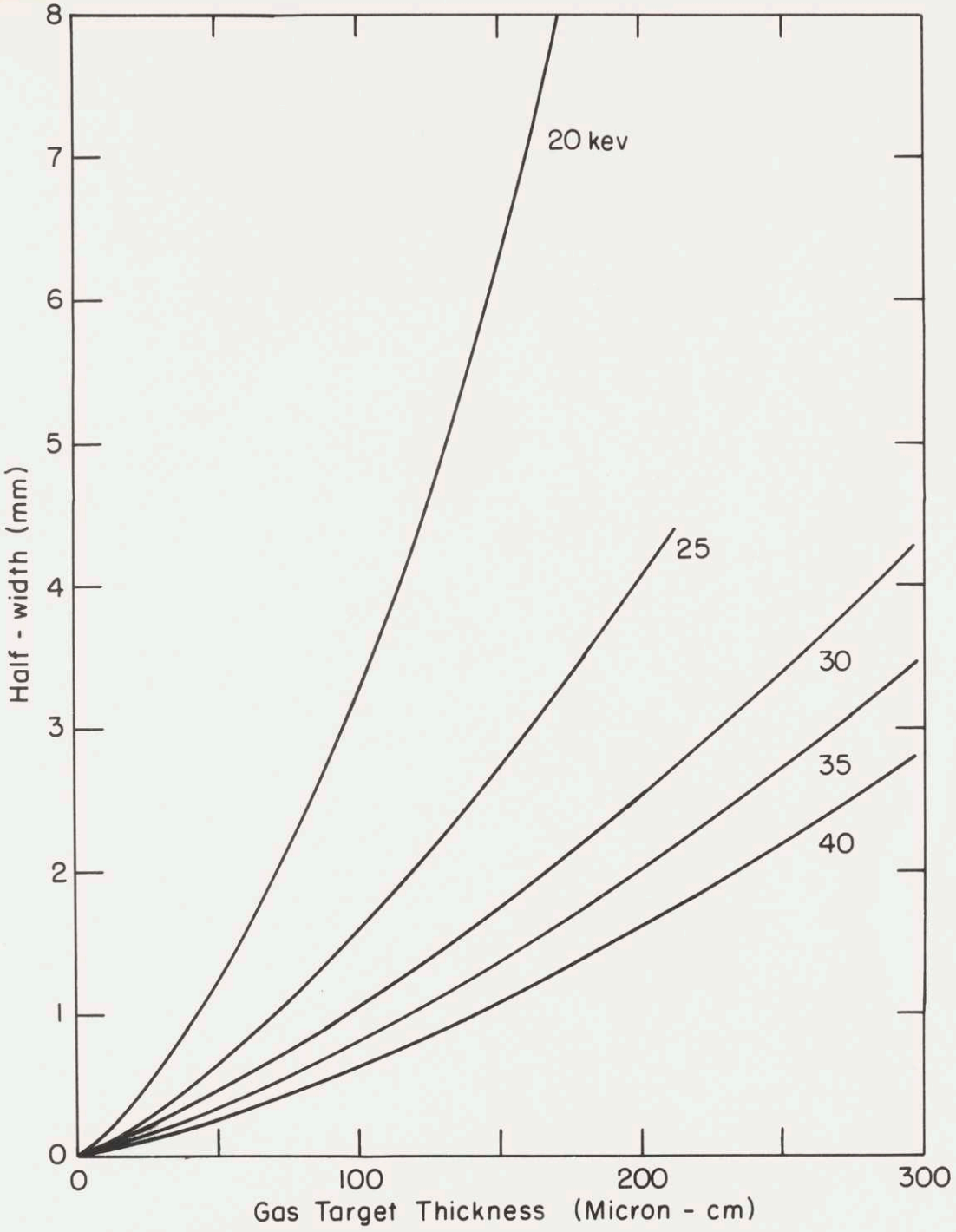

Fig. 3.19 NEON – HELIUM

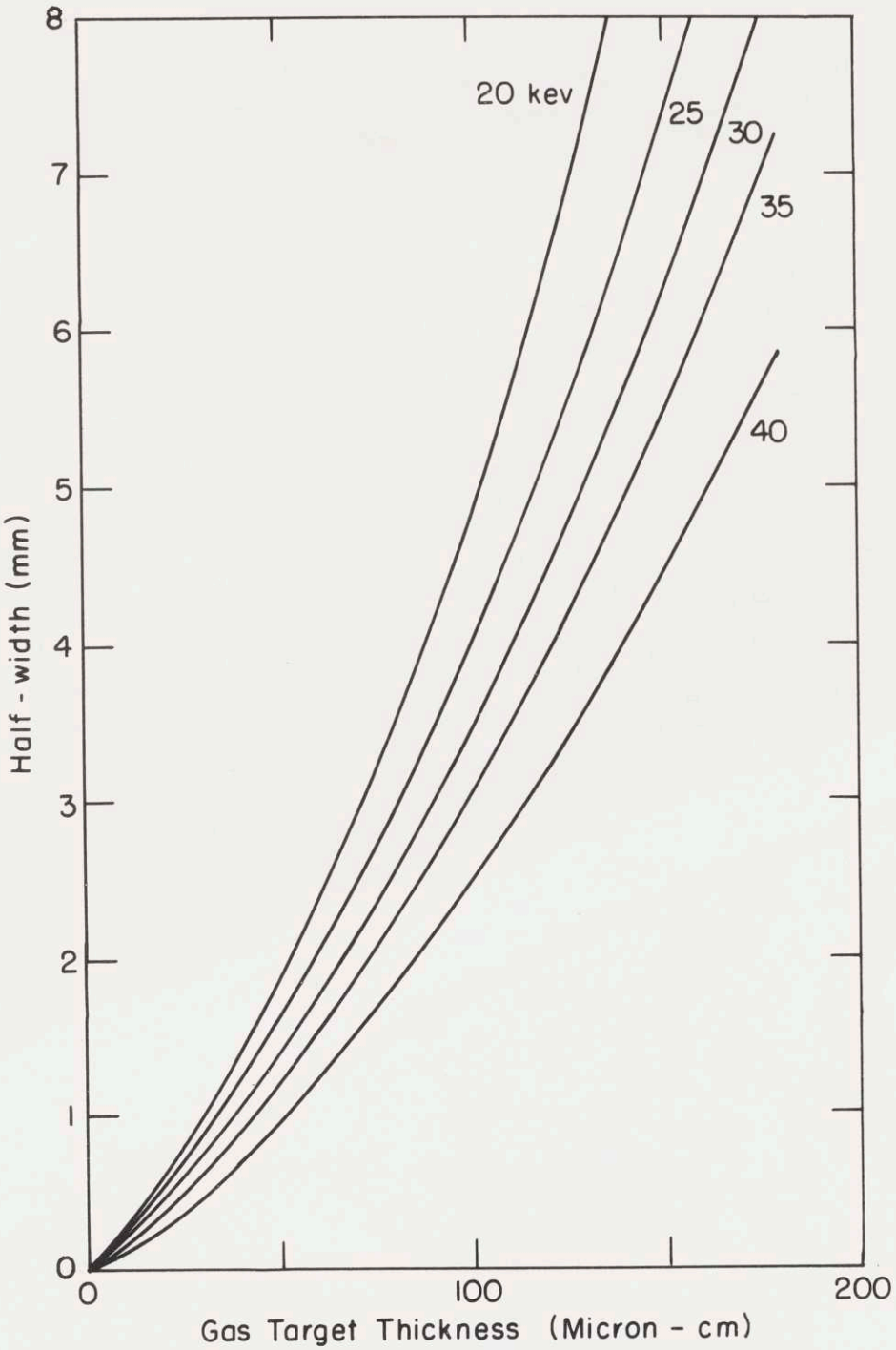

Fig. 3.20 NEON - NEON

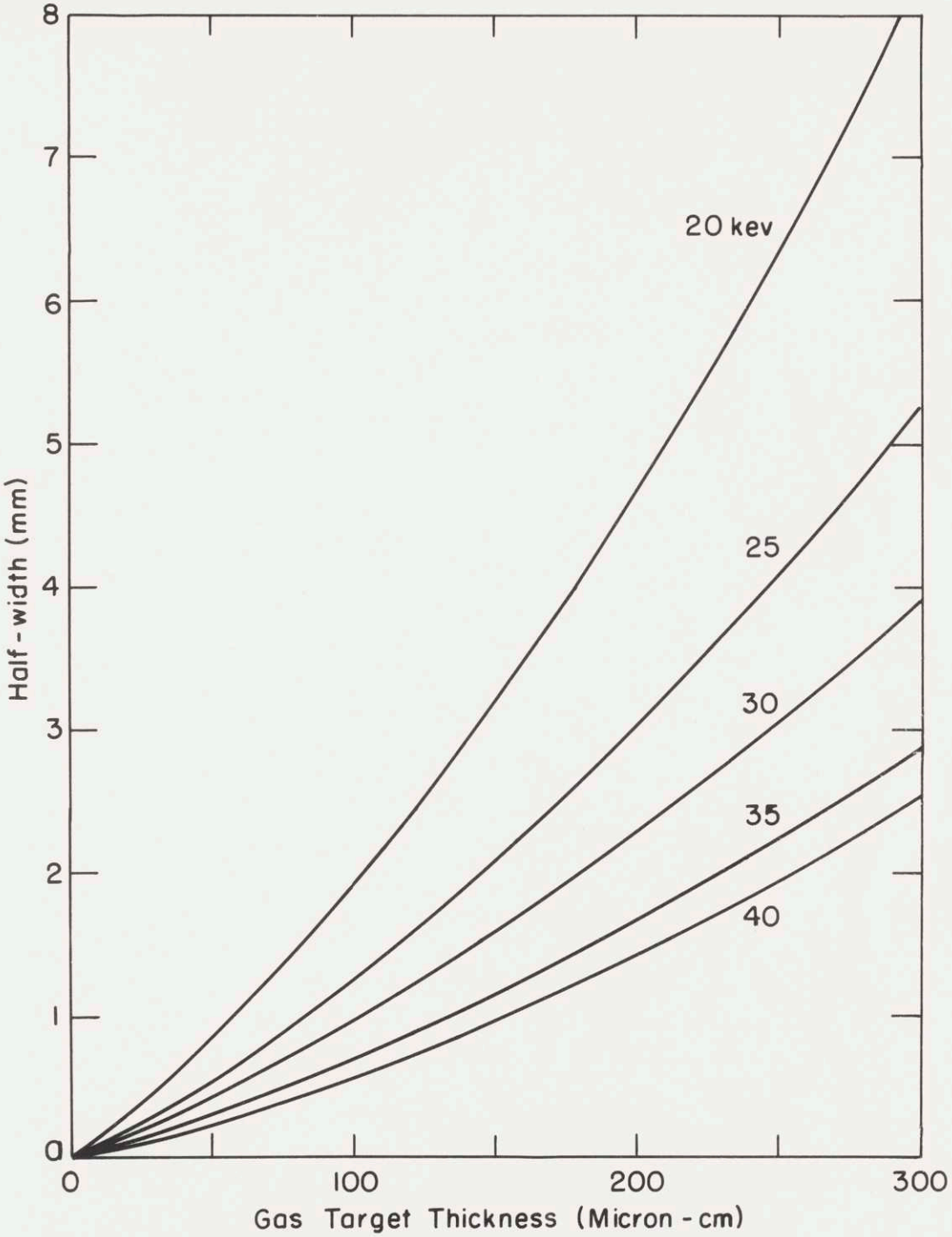

Fig. 3.21 NEON-ARGON

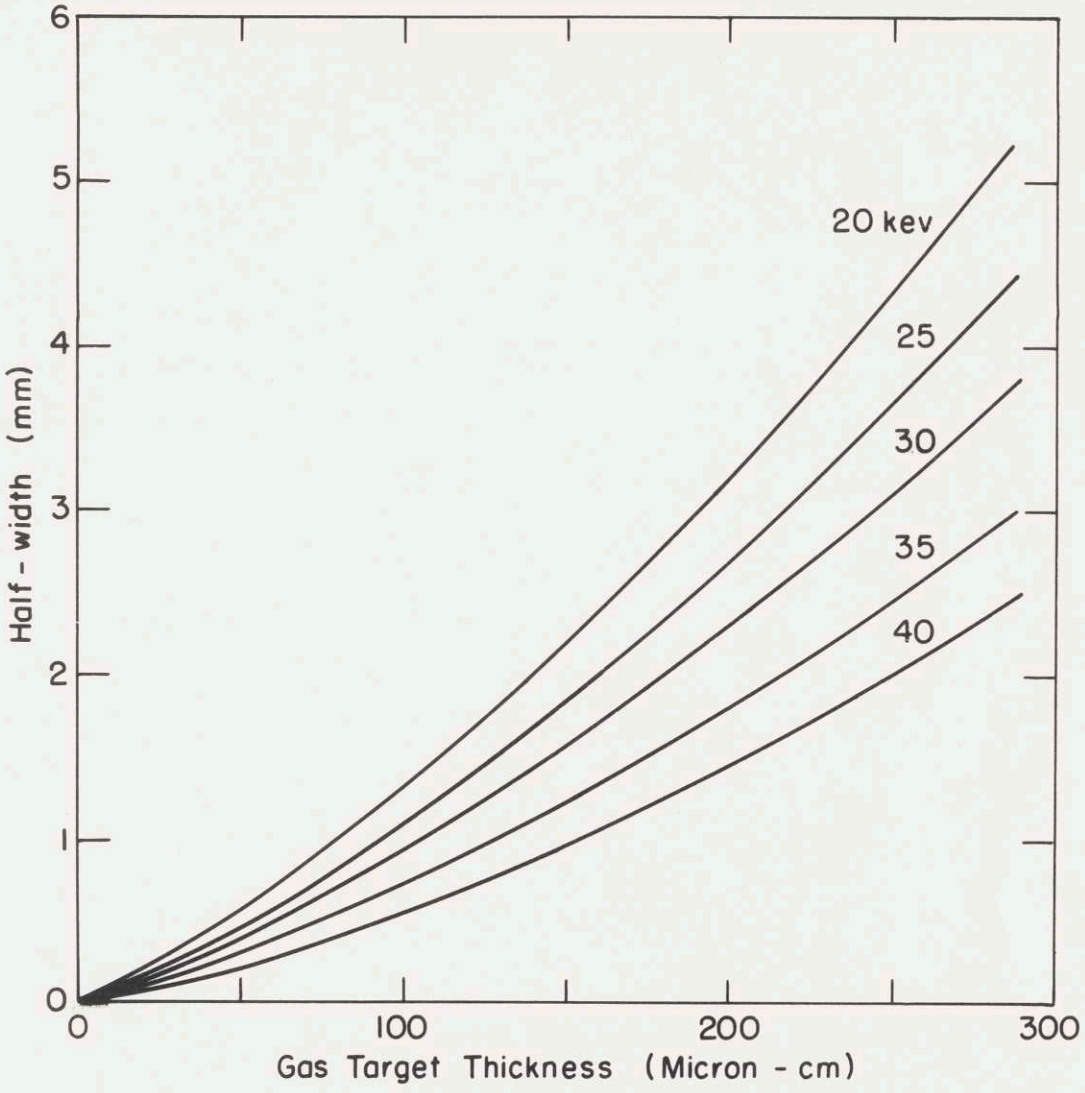

Fig. 3.22 ARGON - HYDROGEN

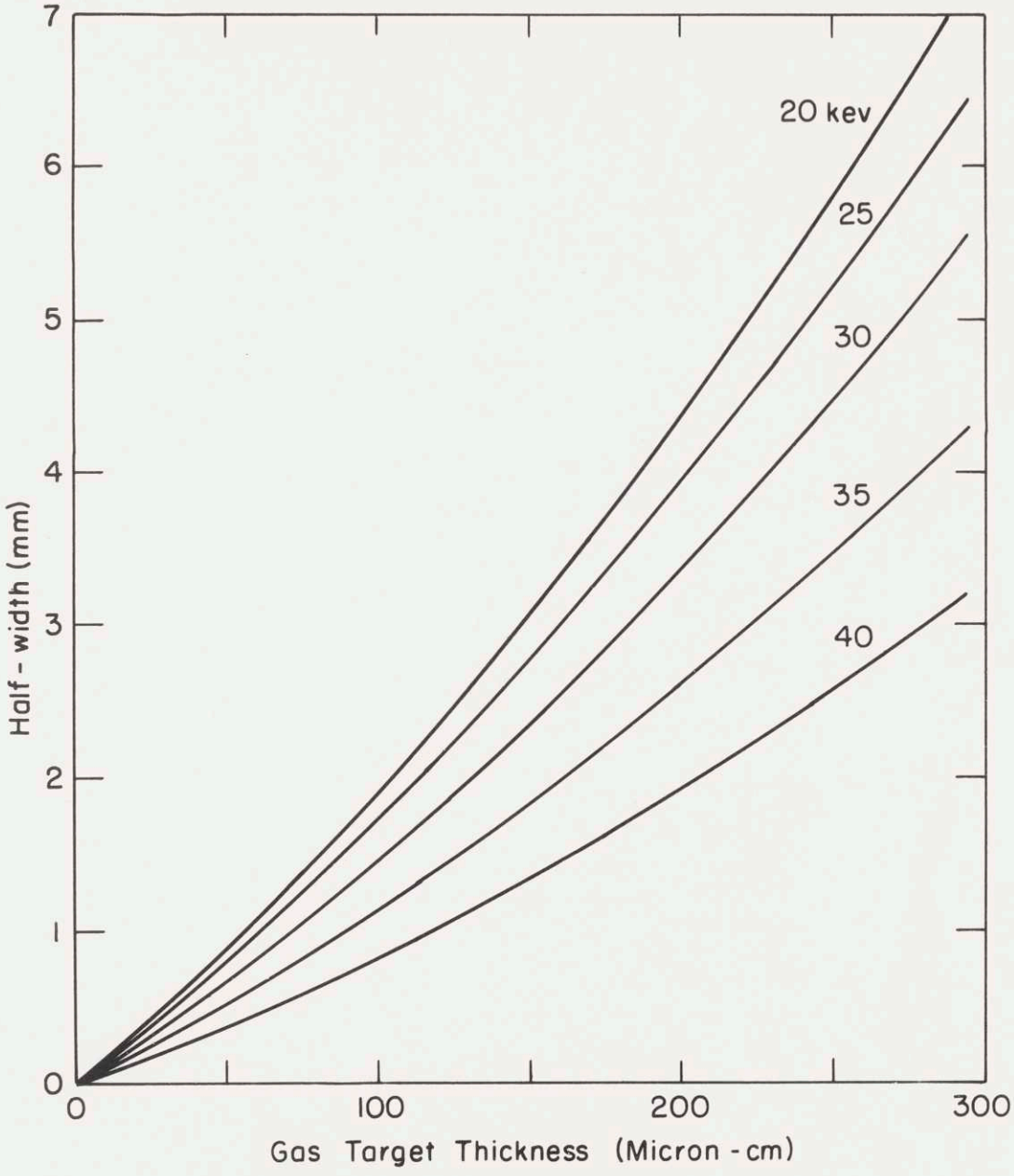

Fig. 3.23 ARGON- HELIUM

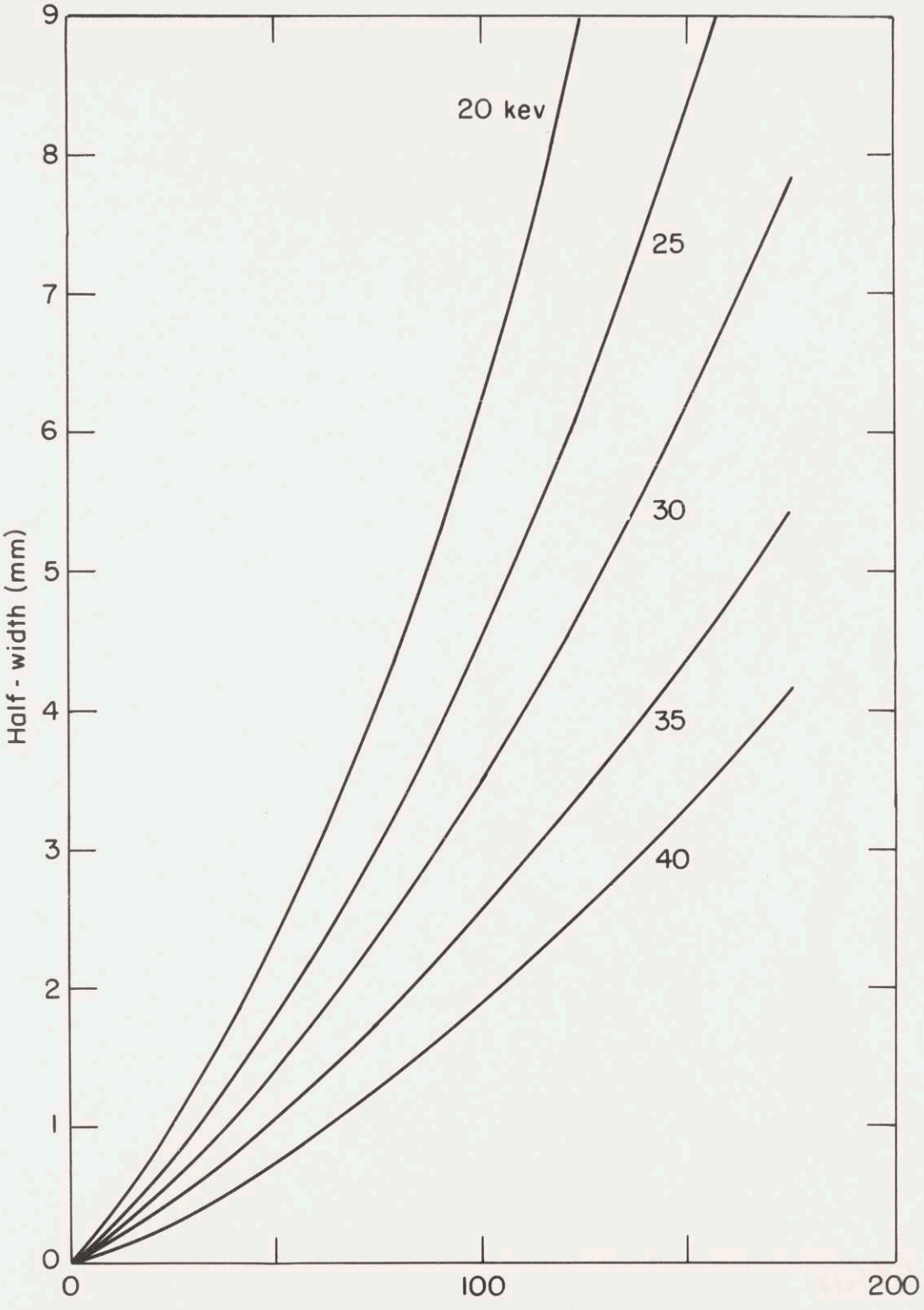

Fig. 3.24 ARGON - NEON

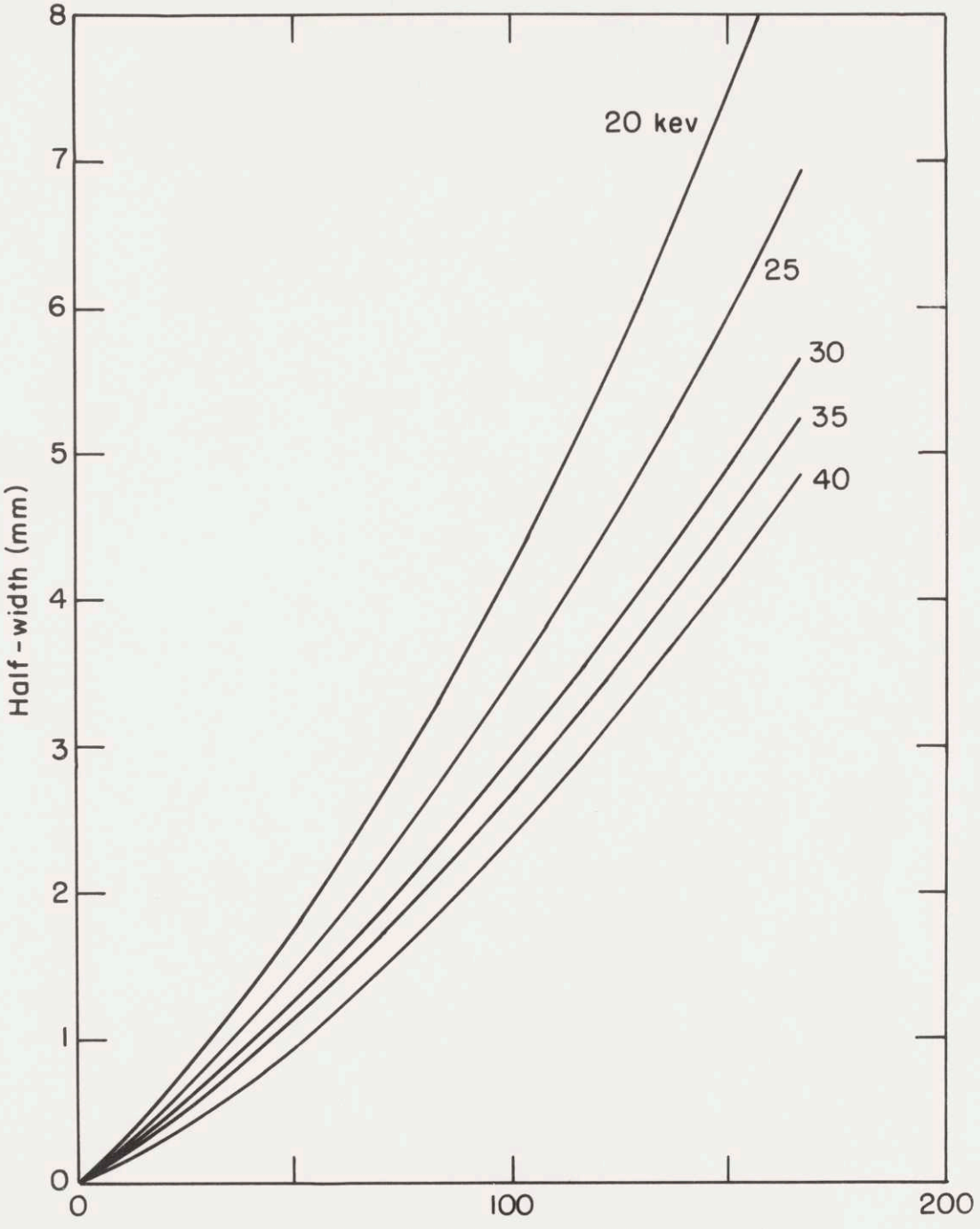

Fig. 3.25 ARGON - ARGON

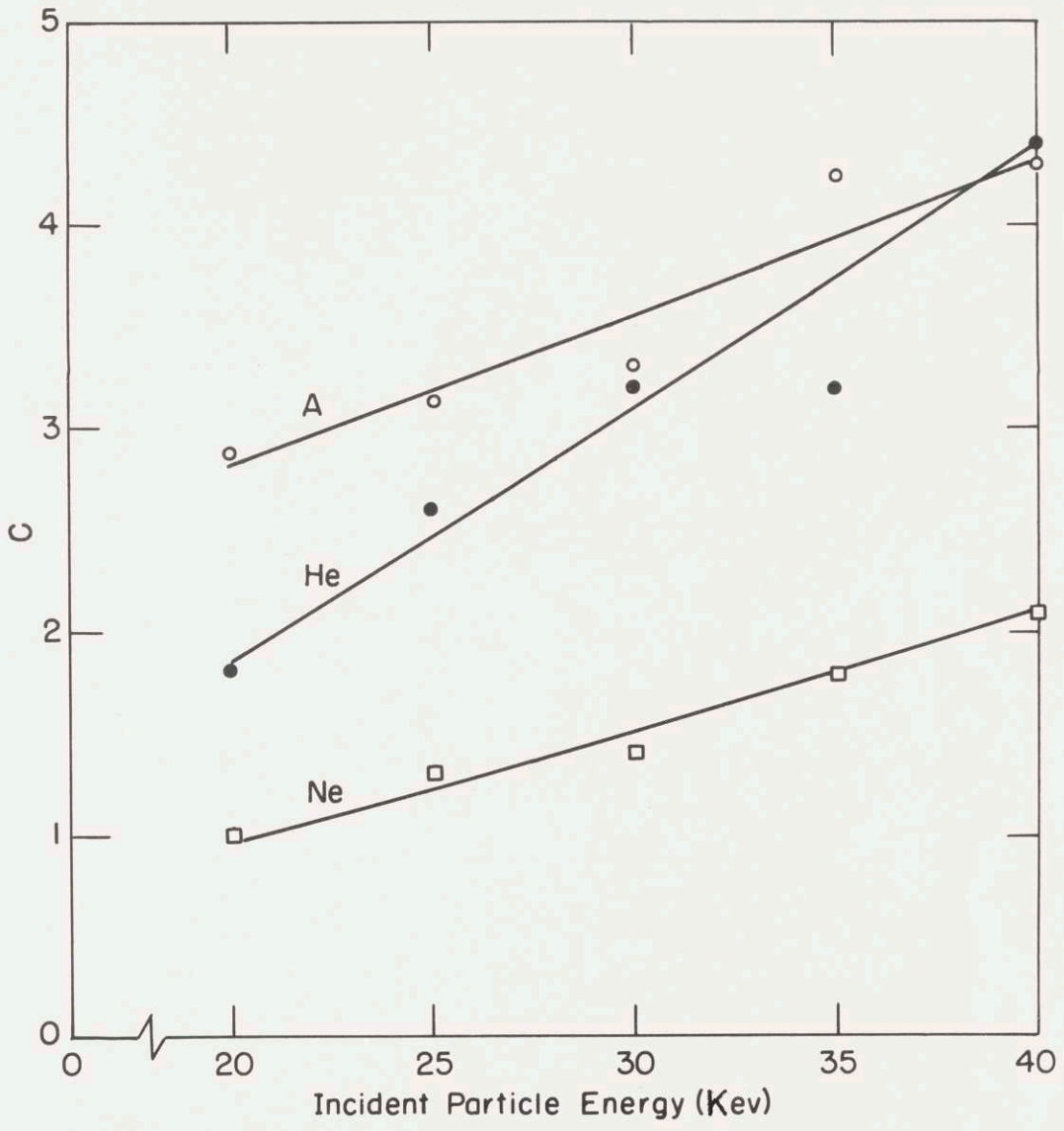

SECONDARY ELECTRON EMISSION COEFFICIENT

Fig. 3.26

CHAPTER IV

INTERPRETATION OF RESULTS

In Chapter Two it was established that we have a Gaussian distribution and that the angle ϕ that includes one-half the scattered particles can be expressed as $\frac{B_0}{L}$, where B_0 is a measured quantity. From equation (2.35) we have

$$\phi = 1.18\,\lambda \tag{4.1}$$

where λ is the most probable angle of deflection. λ then is a function of incident particle energy and mass, target particle mass, and gas target thickness.

$$\lambda = f(E, m_1, m_2, T) \tag{4.2}$$

If we obtain λ from the curves in Figures 3.15 - 3.27 by $\lambda = \frac{B_0}{1.18\,L}$ and plot log λ as a function of log T we obtain straight lines. This tells us that the equations of these lines may be written as

$$\lambda = \beta\, T^{\alpha} \tag{4.3}$$

where α and β are constants for a given straight line; β being the intercept when T = 1 and α being the slope of the line. We can thus obtain an equation giving the relation of λ to T.

These curves were plotted (Figure 4.1 is an example) and values obtained for α and β for the different incident-target combinations. The slope did not change with energy for a given incident-target combination. This indicates that α is not a function of energy but

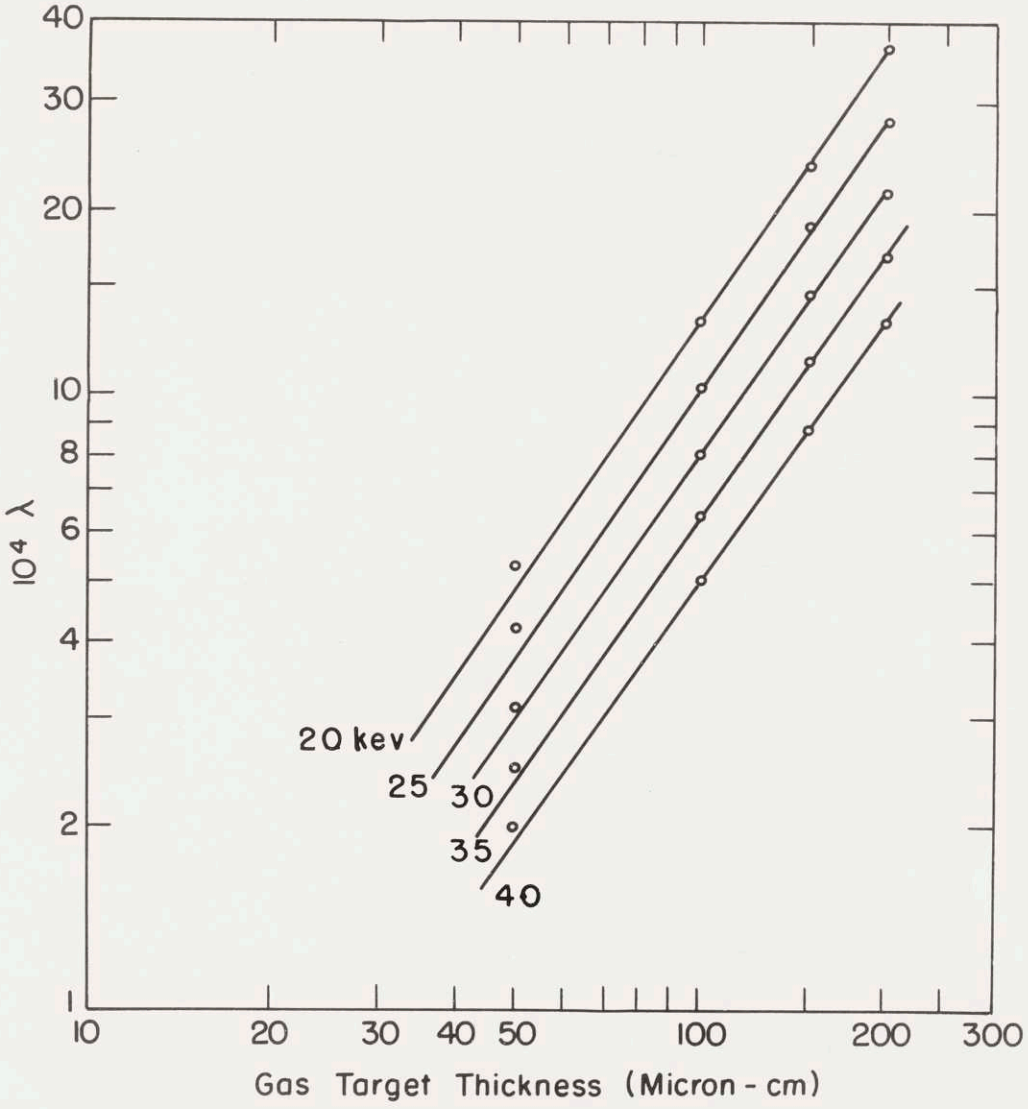

MOST PROBABLE ANGLE OF DEFLECTION AS A FUNCTION OF GAS TARGET THICKNESS

Fig. 4.1

is possibly a function of m_1 and m_2.

$$\alpha = f(m_1, m_2) \tag{4.5}$$

β however changes with energy, indicating that it is a function of energy as well as m_1 and m_2.

$$\beta = f(E, m_1, m_2) \tag{4.6}$$

The exact dependence of α on m_1 and m_2 and β on E, m_1, and m_2 will not be determined in this paper. Figures 4.2, 4.3, and 4.4 show the dependence of β on energy and Figure 4.5 gives a table of the values of α for different incident-target combinations. With β taken from these curves and α from the table, the most probable angle of deflection λ can be found from equation (4.3). With this λ the distribution of the scattered beam can be found at any distance L by

$$\frac{n}{n_T} = 1 - e^{-\frac{r^2}{2B}} \tag{4.7}$$

where $B = \lambda L$ and $\frac{n}{n_T}$ is the fraction of the neutral beam passing through a circle of radius r at a distance L from the scattering target.

A crude check on the validity of equation (4.4) and the accuracy of the experimental data would be to compute the capture cross sections from the scatter data and compare it with published data. We can obtain the capture cross section in the following manner: Calculate the target thickness that gives the critical angle in equation (2.33). This should be the target thickness for one average collision in the target. The capture cross section can then be easily computed. An example of this will be shown for the helium-neon colli-

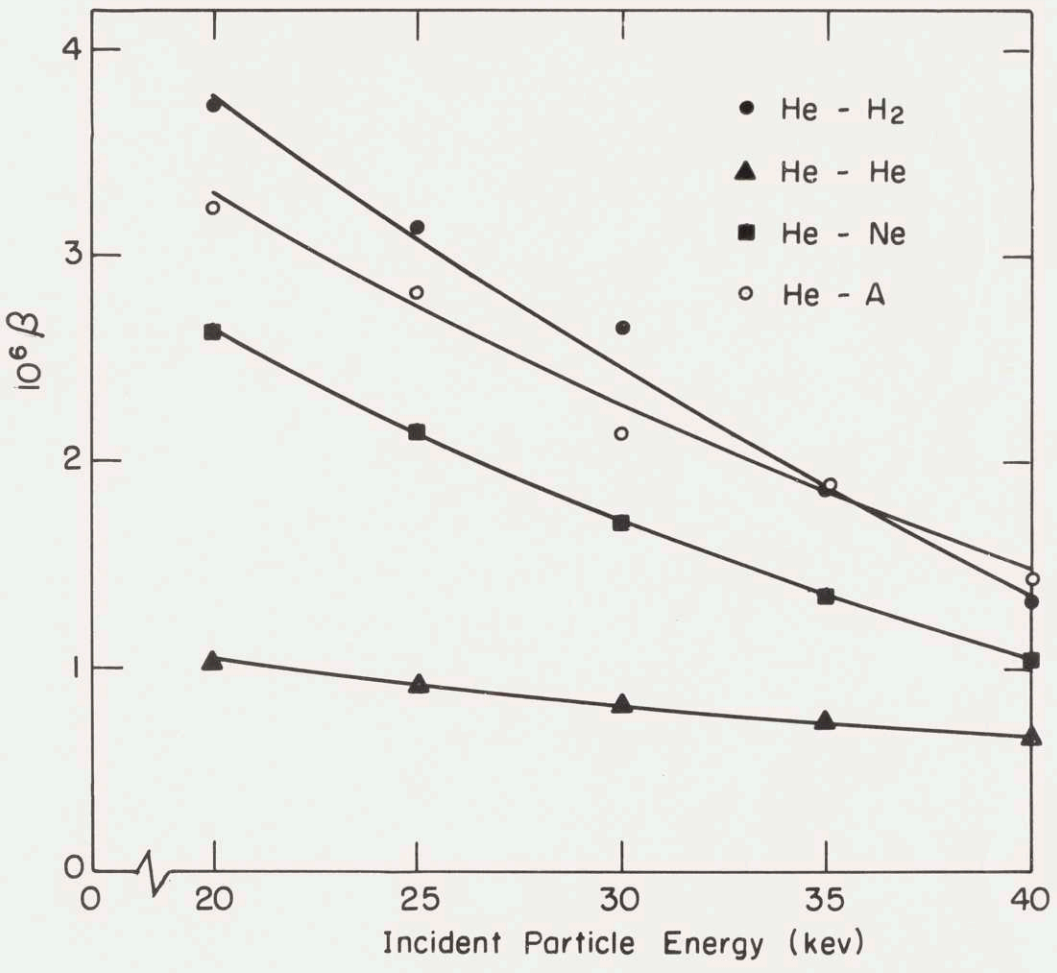

Fig. 4.2 β AS A FUNCTION OF ENERGY WITH HELIUM INCIDENT PARTICLES

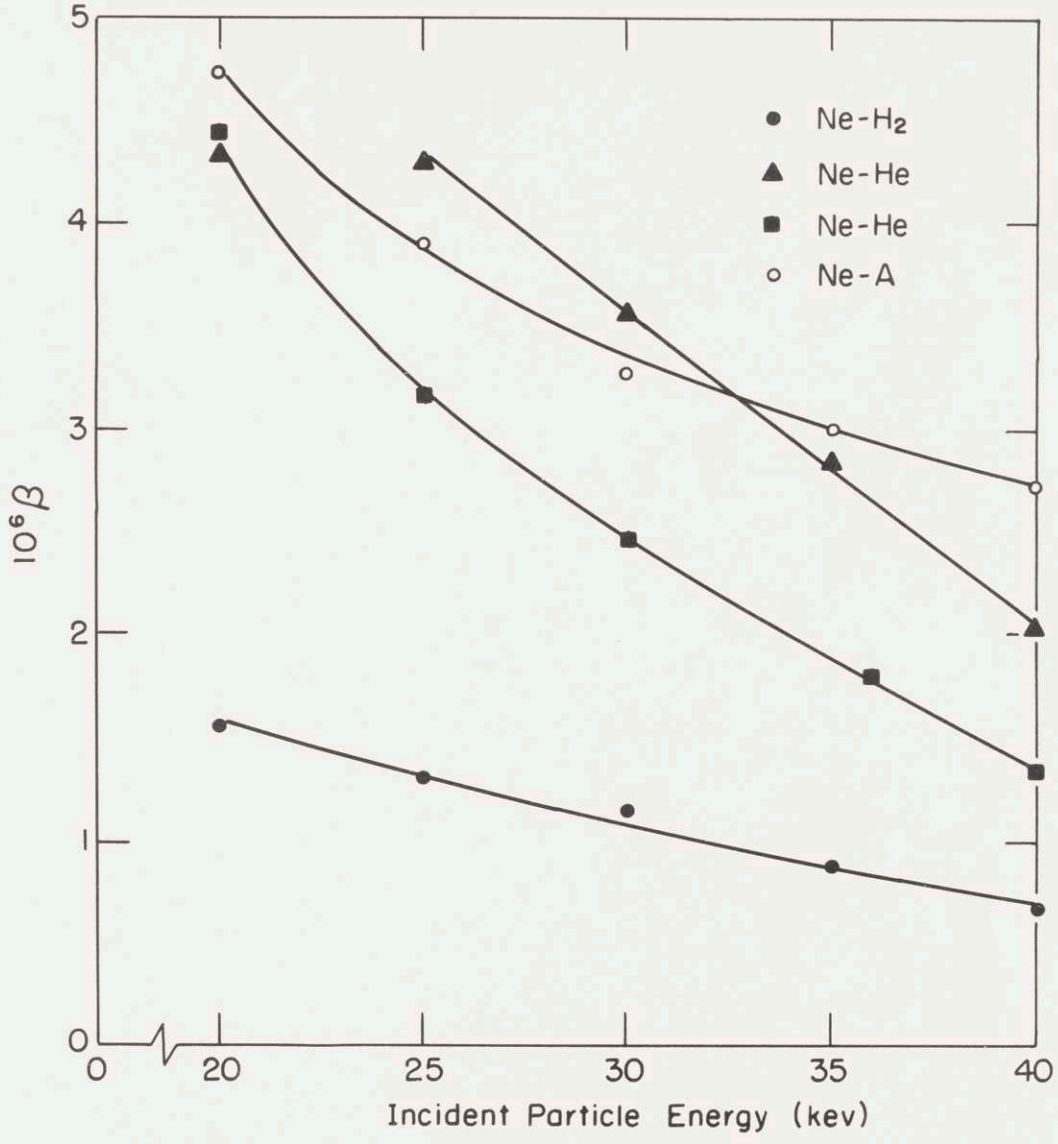

Fig. 4.3 β AS A FUNCTION OF ENERGY WITH NEON INCIDENT PARTICLES

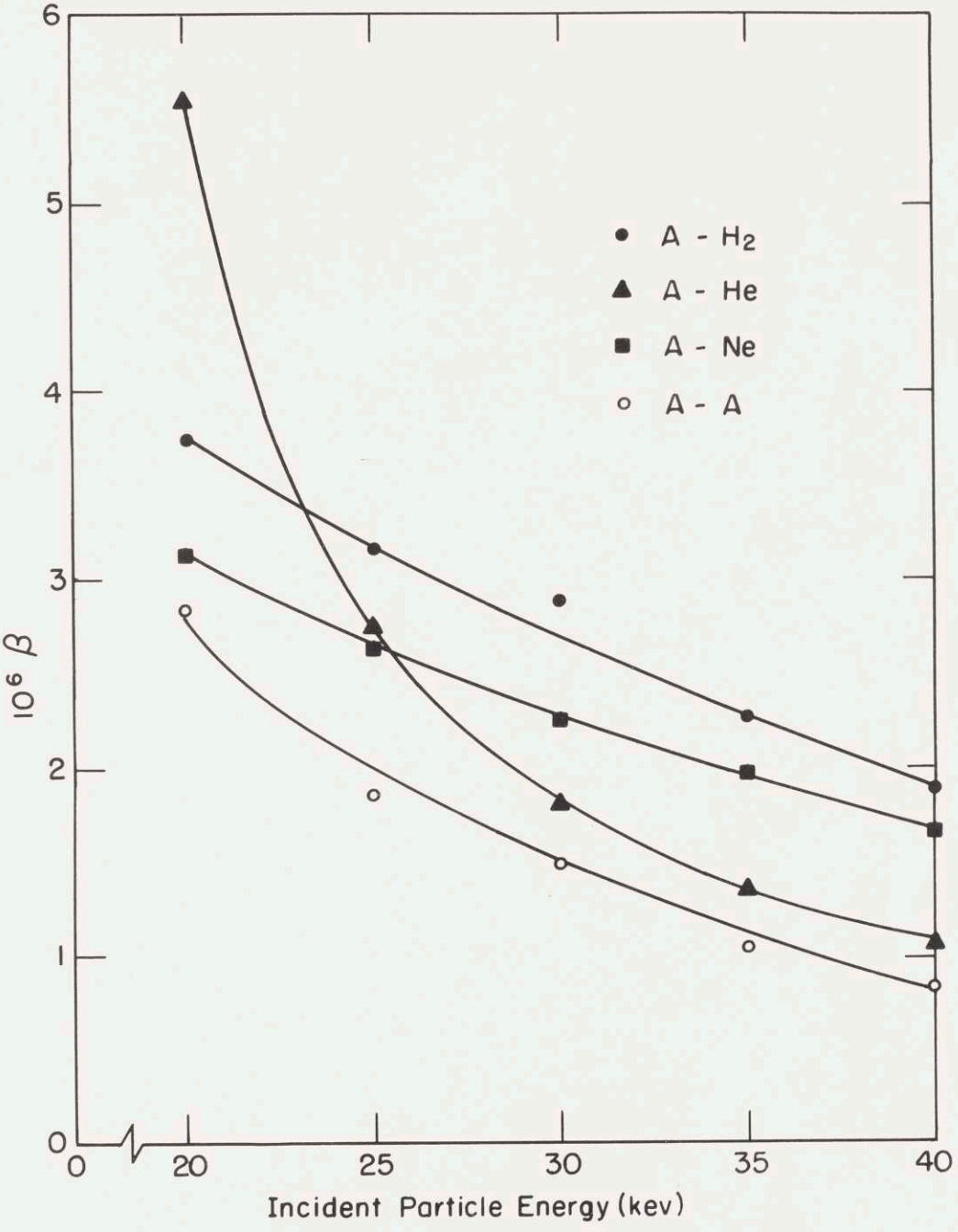

Fig. 4.4 β AS A FUNCTION OF ENERGY WITH ARGON INCIDENT PARTICLES

Incident-target	α
He - H_2	1.18
He - He	1.27
He - Ne	1.35
He - A	1.15
Ne - H_2	1.37
Ne - He	1.26
Ne - Ne	1.47
Ne - A	1.29
A - H_2	1.34
A - He	1.18
A - Ne	1.45
A - A	1.35

Figure 4.5

sion at an incident energy of 30 kev.

The target thickness for a single collision is given by

$$\frac{m_2}{m_1 + m_2}\,\theta_c = \phi = 1.18\,\beta\,T^{\alpha} \tag{4.8}$$

where $\frac{m_2}{m_1 + m_2}$ changes θ_c (equation 2.33) from center-of-mass coordinates to laboratory coordinates. Then for He-Ne at 30 kev

$$4.14 \times 10^{-4} = (1.18)(1.7 \times 10^{-6})\ T^{1.35}$$

$$T = 52 \text{ micron-cm}$$

$$T = (52)(3.56 \times 10^{13}) = 1.85 \times 10^{15} \text{ atoms-cm}^{-2}$$

The defined value for one mean-free-path is the distance an incident ion beam travels in the target until all but $\frac{1}{e}$ of the ions are made neutral atoms. From the relationship of the ion and neutral beams in the gas target

$$n_0 = n_i\,(1 - e^{-\eta x \sigma_{10}}) = n_i\,(1 - e^{-\frac{x}{\lambda_0}}) \tag{4.9}$$

where λ_0 is one mean-free-path and x is the target distance traveled. This neglects the change from neutral to positive charge states which is small in this case. One mean-free-path through the target then occurs when the target length is equal to λ_0 which gives $\frac{n_0}{n_i} = 1 - e^{-1}$. This occurs when $\sigma_{10} = \frac{1}{\eta x} = \frac{1}{T}$. We can now calculate the capture cross section to be $\sigma_{10} = \frac{1}{1.85 \times 10^{15}} = 54 \times 10^{-17} \text{ cm}^2$. From published values of the capture cross section[21], $\sigma_{10} = 50 \times 10^{-17} \text{ cm}^2$. Values of the capture cross section of helium in hydrogen, helium, neon, and argon at 30 kev calculated in this manner gave results that were never off from the published values[21] by

more than a factor of 2. Of course this method cannot be expected to be entirely correct as we use equation (4.4) which is for multiple collisions and force it to the single collision value of equation (2.33). It does, however, indicate that we are obtaining scatter data that, when transformed into charge transfer gives close agreement to published charge transfer measurements.

In the design and operation of equipment using neutral beams it would be very useful to know an optimum beam dispersion and intensity and gas target thickness relationship.

Let us assume a positive ion beam incident upon the gas target with an energy E and an intensity of I_+ amperes. From equation (2.2) the neutral beam current formed will be

$$n_o = I_+ \phi_o \left[1 - e^{-\eta x(\sigma_{01} + \sigma_{10})}\right] \tag{4.10}$$

which can be written as

$$n_o = I_+ \phi_o \left[1 - e^{-KT\sigma}\right] \tag{4.11}$$

where $\sigma = \sigma_{01} + \sigma_{10}$, $K = 3.56 \times 10^{13}$, and T is target thickness measured in micron-cm.

From equation (2.34) we find the number of scattered particles in a cone angle θ to be

$$n = n_o \left(1 - e^{-\frac{\theta^2}{2\lambda^2}}\right) \tag{4.12}$$

which can be written with its target thickness dependence from equation (4.3) as

$$n = n_o \left(1 - e^{-\frac{\theta^2}{2\beta^2 T^{2\alpha}}}\right) \tag{4.13}$$

Then the neutral particle beam intensity contained in a cone angle θ from the incident ion beam I_+ is from equation (4.11) and (4.13)

$$n = I_+ \phi_0 (1 - e^{-K T \sigma})(1 - e^{-\frac{\theta^2}{2\beta^2 T^2 \alpha}}) \qquad (4.14)$$

A specific machine design would somewhat fix the allowable maximum angle of scatter. We could then find a target thickness for maximum neutral current through a given angle θ by differentiating equation (4.14) with respect to T, setting equal to zero, and solving for T. This is a complex problem and cannot be done by simple straightforward mathematics.

A solution can be obtained, however, by graphical methods. The results of solutions for He-He at 20 kev and at 40 kev are given as an example and were obtained in the following manner. Equation (4.14) was solved (using values of σ given by Allison[21], and values for β and α given in Figures 4.2 and 4.5 respectively) for angles of $\theta = 10^{-4}$, 2×10^{-4}, 3×10^{-4}, and 4×10^{-4} radians, and values of T from 30 to 110 micron-cm. n as the percentage of I_+ was then plotted for the four θ values as a function of T. These plots are given in Figure 4.6 for 20 kev and Figure 4.7 for 40 kev. Then in Figure 4.8 θ is plotted as a function of the target thickness where the maximum occurs. These points plot into straight lines on semilogarithmic paper which is not surprising from the exponential nature of equation (4.14). From these curves we can obtain the desired relation between gas target thickness and the angular spread of the beam as

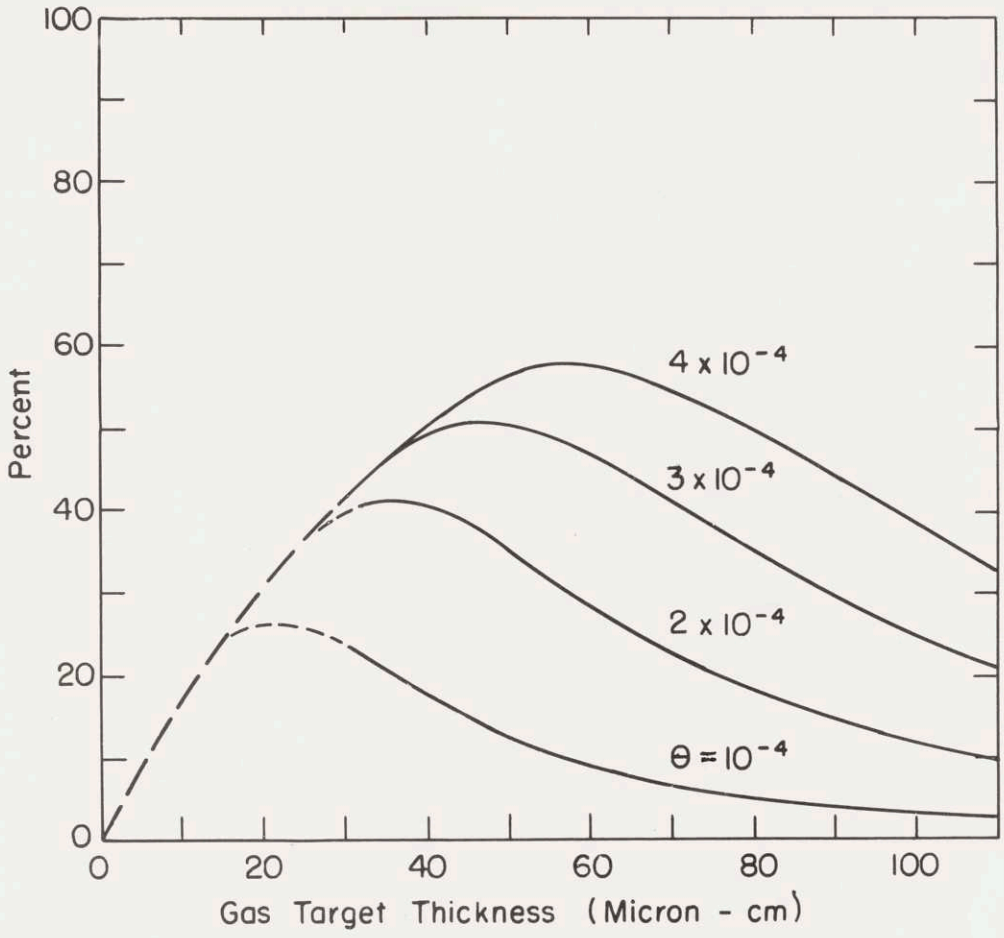

PERCENTAGE OF INCIDENT 20 kev HELIUM ION BEAM NEUTRALIZED AND CONTAINED IN GIVEN CONE ANGLE AS A FUNCTION OF HELIUM GAS TARGET THICKNESS.

Fig. 4.6

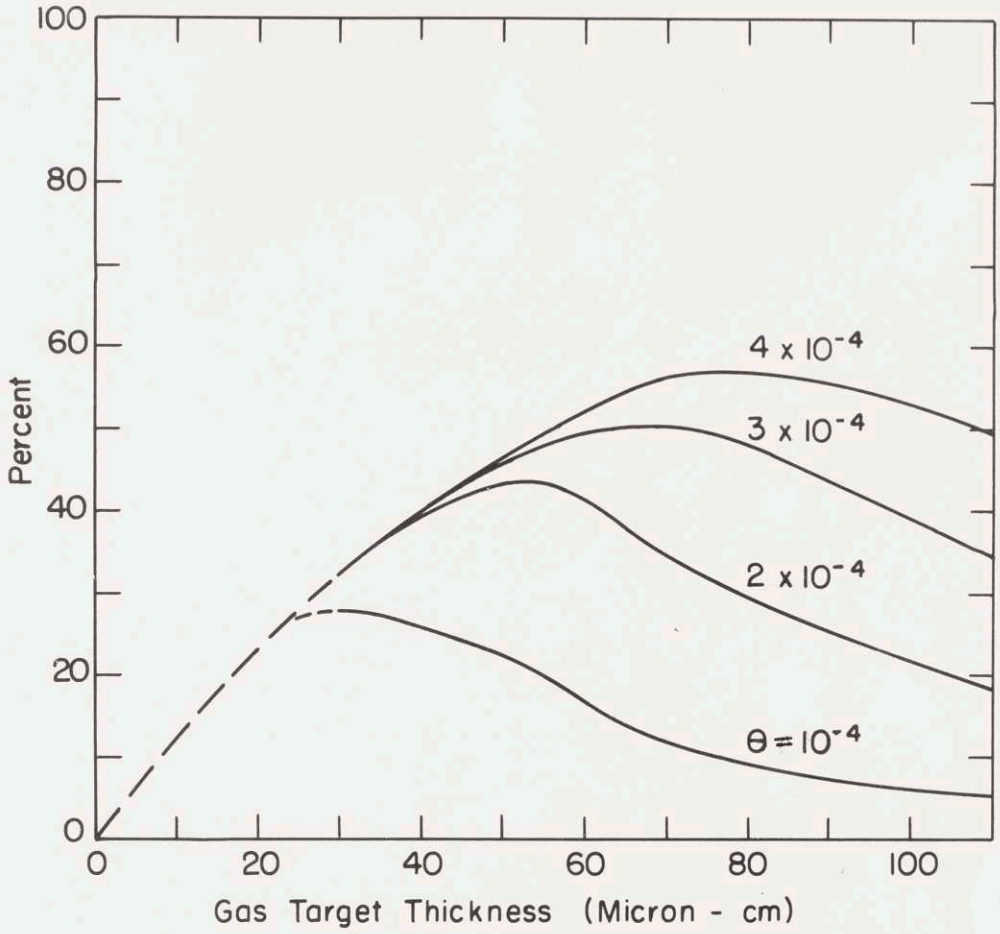

PERCENTAGE OF INCIDENT 40 kev HELIUM ION BEAM NEUTRALIZED AND CONTAINED IN GIVEN CONE ANGLE AS A FUNCTION OF HELIUM GAS TARGET THICKNESS

Fig. 4.7

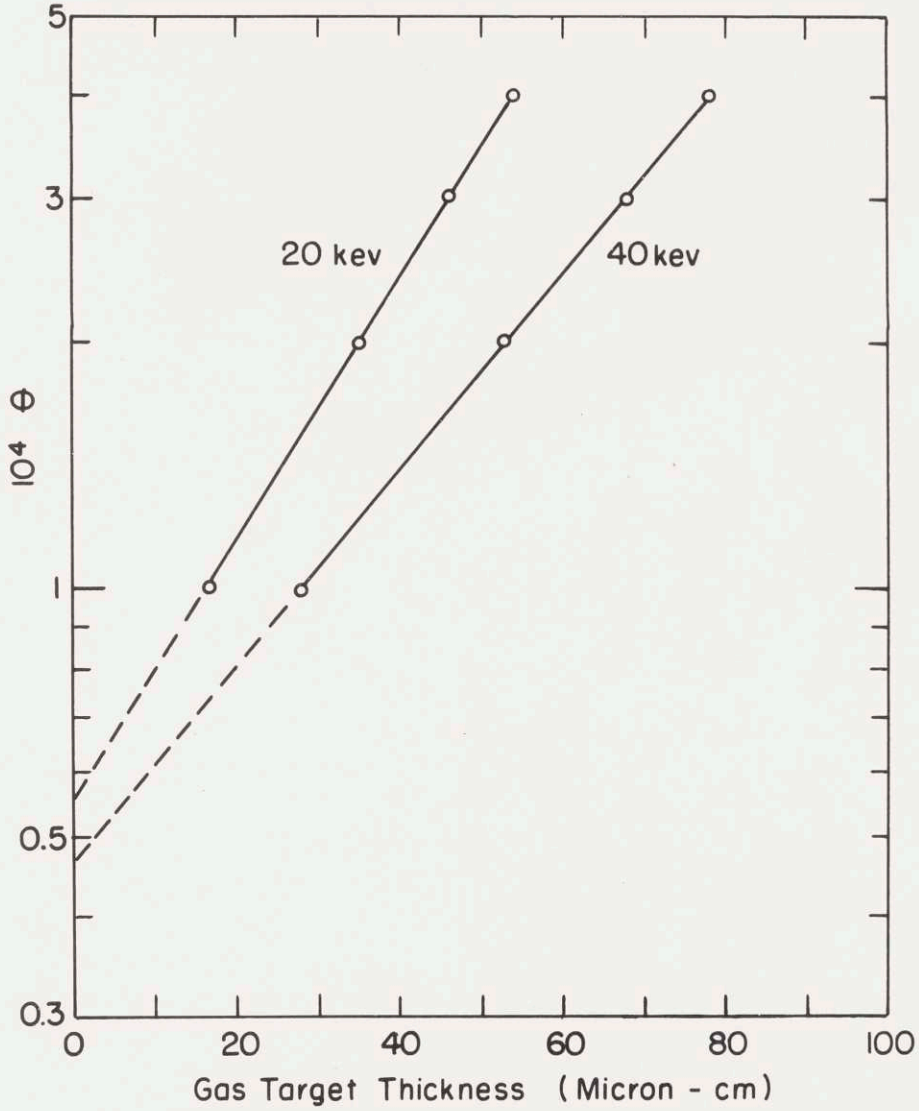

CONE ANGLE AS A FUNCTION OF THE TARGET THICKNESS FOR MAXIMUM NEUTRALS IN THE CONE ANGLE.

Fig. 4.8

$$T = 27.2 \ln\left(\frac{\theta}{5.55 \times 10^{-5}}\right) \qquad \text{(4.14 a) 20 kev}$$

$$T = 36 \ln\left(\frac{\theta}{4.6 \times 10^{-5}}\right) \qquad \text{(4.14 b) 40 kev}$$

These equations give the target thickness in micron-cm that will give the maximum neutral particle current in a given cone angle θ from an incident positive ion beam.

Clearly the energy dependence of the constants in equations 4.14 a and 4.14 b could be obtained by obtaining the equations for other energies but due to the formidable amount of calculations involved such an undertaking will not be attempted in this paper.

In summary it should be stressed again that the results obtained in this paper have been with the assumption that the ion beam enters the charge transfer target focused such that it would come to a point at the neutral beam target neglecting coulomb repulsive forces. There are two discrepancies in this assumption. First, the repulsive forces are present but if the density of the beam is relatively low and the gas target is relatively short and near the focusing section, these forces possibly may be neglected. Second, the ion optical system is never perfect and due to aberration and/or astigmatism of the focusing system, a finite spot would be observed even without the coulomb repulsive forces. It is believed that both these discrepancies would be constant for a given set of conditions and could be added in as such and would not

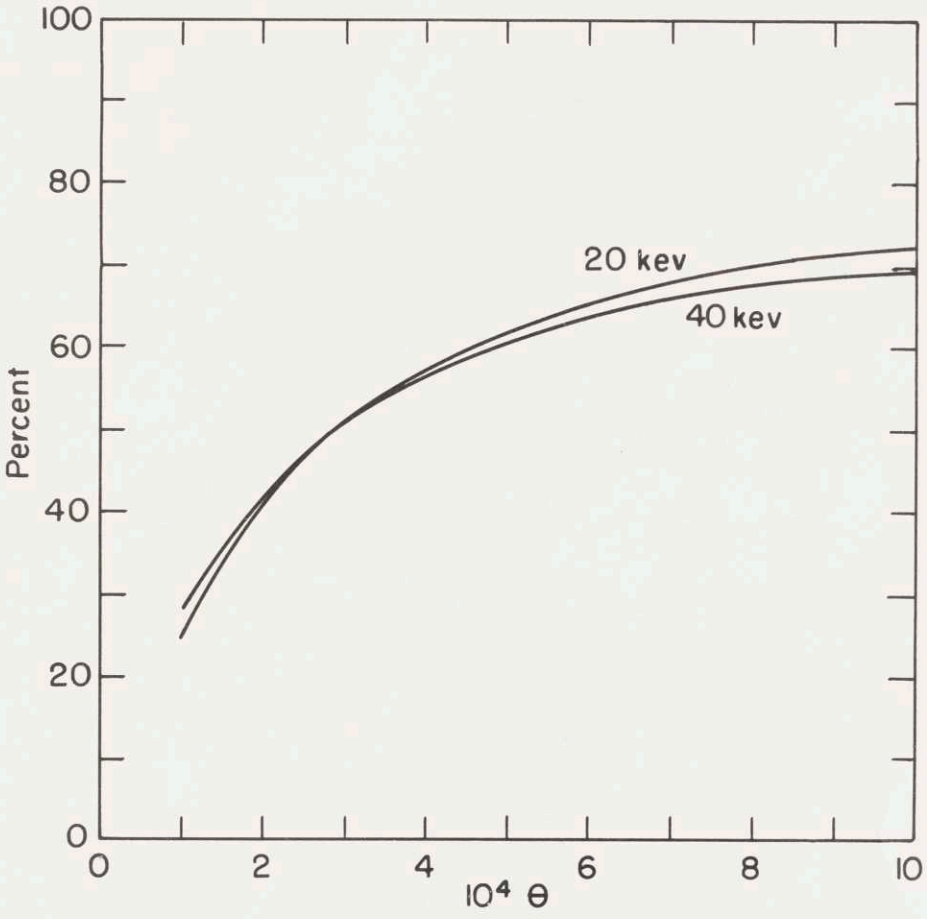

PERCENTAGE OF THE INCIDENT HELIUM ION BEAM NEUTRALIZED AND CONTAINED IN THE CONE ANGLE, θ

Fig. 4.9

affect the validity of the results of this paper.

With the results given in this paper then, taking account of the constant discrepancies, the behavior of a neutral beam could be accurately predicted and its optimum operating points determined.

From Figure 4.9 the percentage of the incident ion beam resulting in neutrals contained in a given cone angle varies but very little from 20 to 40 kev, indicating that in an actual machine design the determination of the incident ion energy could be left to optimum source and beam forming conditions and the gas target thickness could be adjusted for nearly the same maximum at any voltage.

REFERENCES

1. L. Dunoyer, Compt. rend. 152, 592 (1911)
2. K. F. Smith, Molecular Beams, John Wiley and Sons, New York (1955)
3. O. Stern and W. Garlach, Ann. Physik, 74, 673 (1924)
4. I. Estermann, R. Frisch, and O. Stern, Zeit. f. Physik, 73, 348 (1931)
5. I. I. Rabi, Phys. Rev., 51, 652 (1937)
6. H. S. W. Massey and C. B. O. Mohr, Proc. Roy. Soc., A 144, 188 (1934)
7. M. L. E. Oliphant, Proc. Roy. Soc., A 124, 228 (1929)
8. O. Beeck, Ann. der Phys. (5) 19, 121 (1934)
9. H. Bartels, Ann. der Phys., 13, 373 (1932)

   R. A. Smith, Proc. Camb. Phil. Soc., 30, 514 (1934)

   F. Goldmann, Ann. der Phys., 10, 460 (1931)

   J. P. Keene, Phil. Mag., 40, 369 (1949)

   H. Meyer, Ann. der Phys., 30, 635 (1937)

   A. C. Whittier, Can. Journal Phys., 32 #4, 275 (1954)

   J. H. Montague, Phys. Rev., 81 #6, 1026 (1951)

   S. F. Philp, Ph.D. Thesis, Physics, M.I.T. (1958)
10. R. J. Van de Graaff, Personal conversation
11. L. I. Schiff, Quantum Mechanics, McGraw-Hill, (1949) Chapter V
12. L. I. Schiff, Quantum Mechanics, Chapter VII
13. S. F. Philp, Ph.D. Thesis, Physics, M.I.T. (1958)
14. W. Bothe, Handbuch d. Phys., 22 #2, 1 (1933)
15. F. Jorgensen, Jr., C. E. Knyatt, W. W. Lang, and C. A. Sautter, Paper presented at the 1959 Winter Meeting of the American Physical Society at California Tech.

16. S. Dushman, Scientific Foundations of Vacuum Technique, Wiley (1949) Section 10

17. F. Soddy and A. Berry, Proc. Roy. Soc. 83, 254 (1910)

18. I. Amdur and H. Pearlmann, Rev. Sci. Inst., 10, 174 (1939)

I. Amdur and C. F. Glick, Rev. Sci. Inst., 16, 117 (1945)

19. H. Meyer, Ann. der Physik, 30, 635 (1937)

H. Wayland, Phys. Rev., 52, 31 (1937)

20. R. S. Burington, Handbook of Mathematical Tables and Formulas, Handbook Publishers (1940), Page 255

21. S. K. Allison, Revs. Mod. Phys., 30, 1109 (1958)